X-ray polarization from magnetar sources

IASF-MI Seminar
April 10, 2024

IXPE Imaging X-Ray Polarimetry Explorer

Neutron stars: general notions

- Neutron stars (NSs) are relics of massive stars ($M_{\mathrm{prog}} \approx 8 - 25\ M_{\odot}$)
- Masses $M_{\mathrm{NS}} \approx 1 - 2\ M_{\odot}$
- Radii $R_{\mathrm{NS}} \approx 10 - 15\ \mathrm{km}$

$\rho_{\mathrm{m}} \approx 10^{14} - 10^{15}\ \mathrm{g/cm^3}$

- Sustained by the pressure of degenerate neutrons

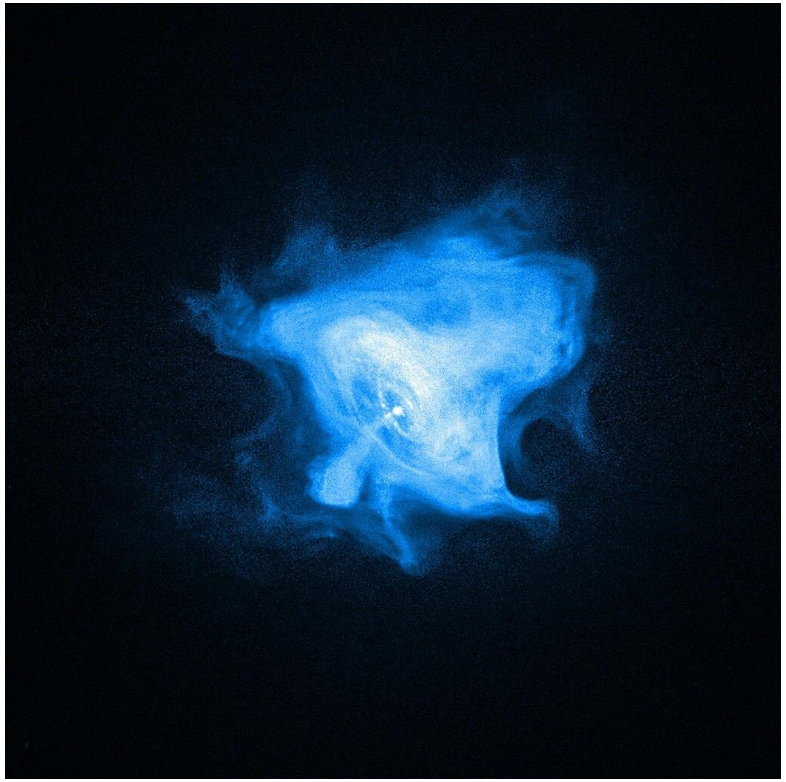

Neutron stars: general notions

- Neutron stars (NSs) are relics of massive stars ($M_{\mathrm{prog}} \approx 8 - 25\ M_{\odot}$)
- Masses $M_{\mathrm{NS}} \approx 1 - 2\ M_{\odot}$
- Radii $R_{\mathrm{NS}} \approx 10 - 15\ \mathrm{km}$

$\rho_{\mathrm{m}} \approx 10^{14} - 10^{15}\ \mathrm{g/cm^3}$

- Sustained by the pressure of degenerate neutrons
- Fast rotators

$$P \approx 10^{-2} - 10\ \mathrm{s}$$
$$\dot{P} \approx 10^{-20} - 10^{-9}\ \mathrm{s/s}$$

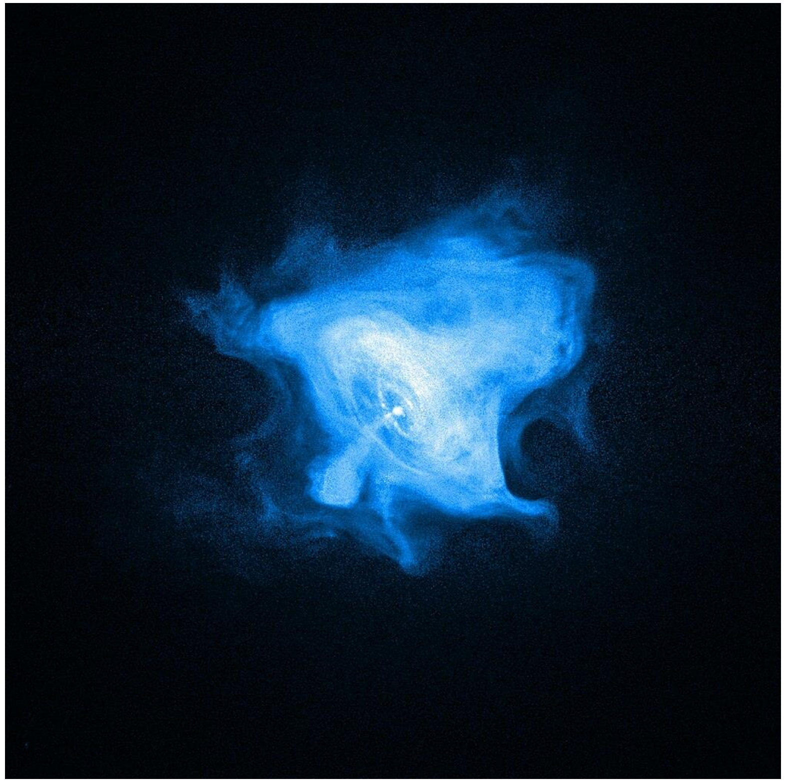

Neutron stars: general notions

- Neutron stars (NSs) are relics of massive stars ($M_{\rm prog} \approx 8 - 25\ M_\odot$)
- Masses $M_{\rm NS} \approx 1 - 2\ M_\odot$
- Radii $R_{\rm NS} \approx 10 - 15\ \mathrm{km}$

$\rho_{\rm m} \approx 10^{14} - 10^{15}\ \mathrm{g/cm^3}$

- Sustained by the pressure of degenerate neutrons
- Fast rotators
- Powerful magnets

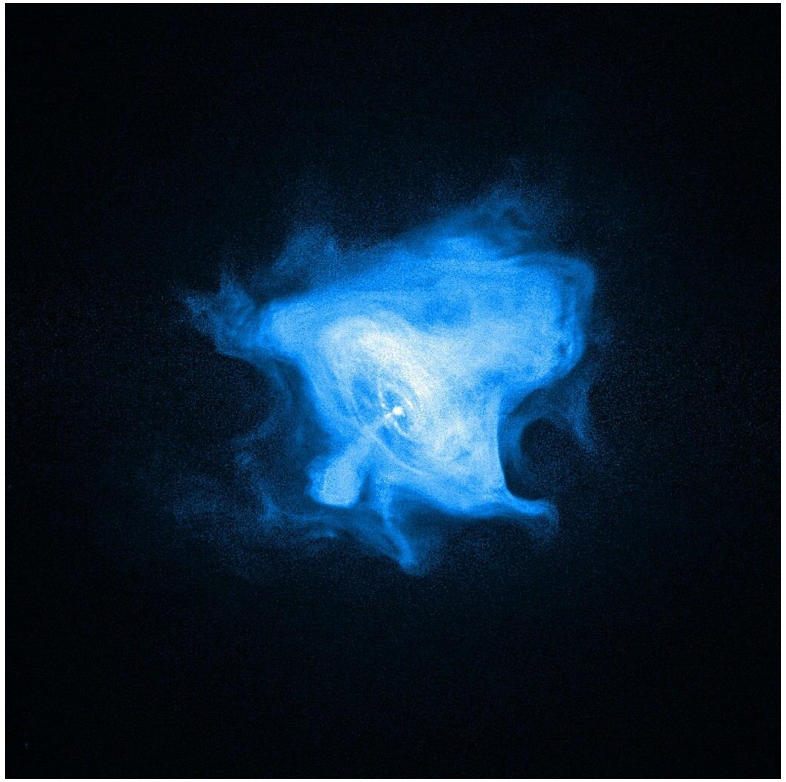

Magneto-rotational evolution

- A rotating dipole field emits EM radiation at the expenses of the rotational energy

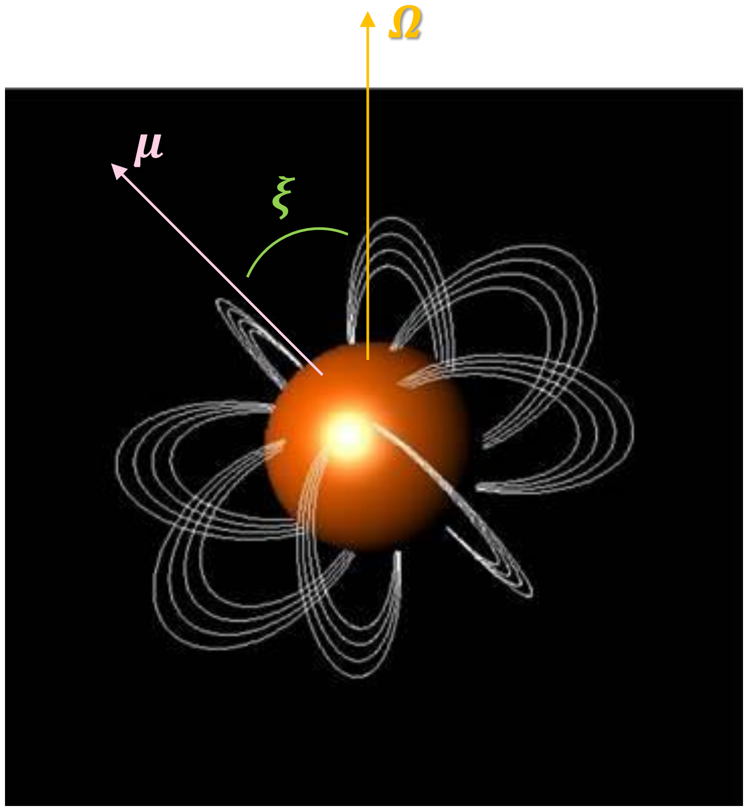

Larmor formula

$$-\frac{2}{3c^3}\left(\frac{\partial^2 \mu}{\partial t^2}\right)^2 = I\Omega\dot{\Omega}$$

Magnetic dipole moment

Rotation frequency ($\Omega = 2\pi/P$)

Magneto-rotational evolution

- A rotating dipole field emits EM radiation at the expenses of the rotational energy

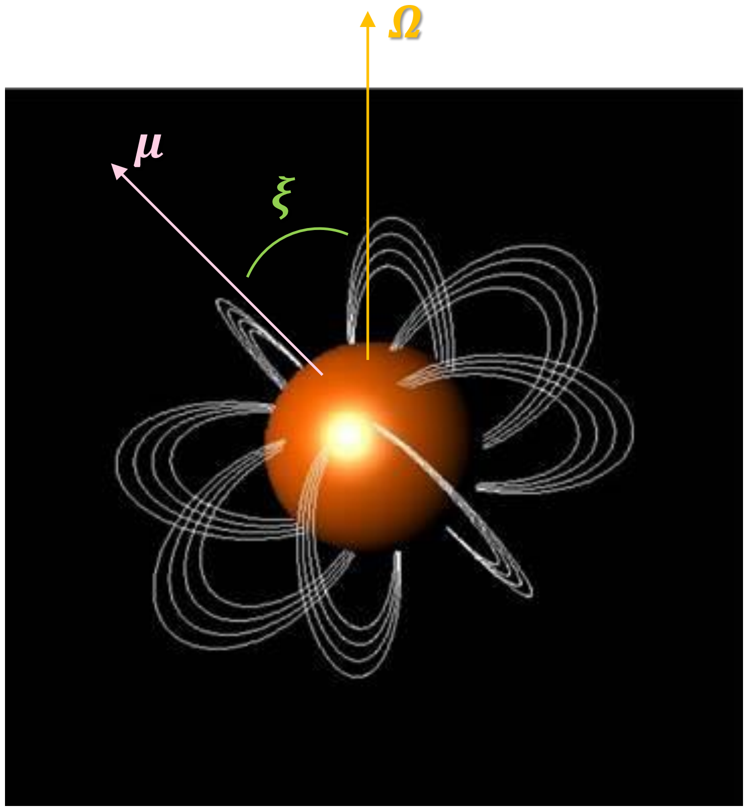

Solving for B

$$B \approx 3.2 \times 10^{19} \sqrt{P\dot{P}}\ \mathrm{G}$$

This holds for:

- purely dipolar magnetic field ($\boldsymbol{\mu}$ in the Larmor formula)
- all the rotation energy is converted into EM emission

Introduction

- Focus on persistent magnetar sources
- Isolated neutron stars
- P-$\dot{P}$ estimate of the magnetic field strength
  $B \approx 10^{14} - 10^{15}$ G
- Observationally identified as AXPs and SGRs
- $L_X > I\Omega\dot{\Omega} \;\; \Rightarrow$ Internal magnetic energy
- Properties of AXPs and SGRs are shared between the two classes (magnetars)

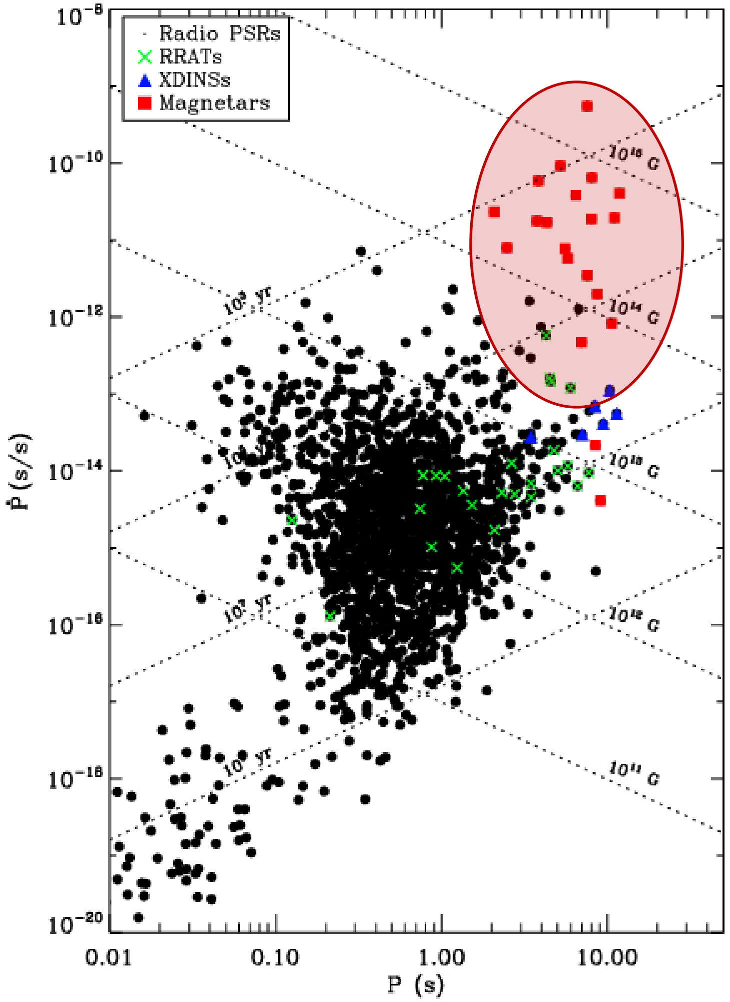

Spectral properties

- Soft X-ray spectra ($0.5\text{–}10\ \mathrm{keV}$) usually fitted by BB+PL decomposition (alternative BB+BB, especially for transients in outburst)
- Typical $kT_{\mathrm{BB}} \approx 0.3\text{–}0.5\ \mathrm{keV}$ and $\Gamma_{PL} \approx -(2\text{–}4)$ dominating above $\approx 3\text{–}4\ \mathrm{keV}$
- Additional PL component at higher energies ($\gtrsim 20\ \mathrm{keV}$)

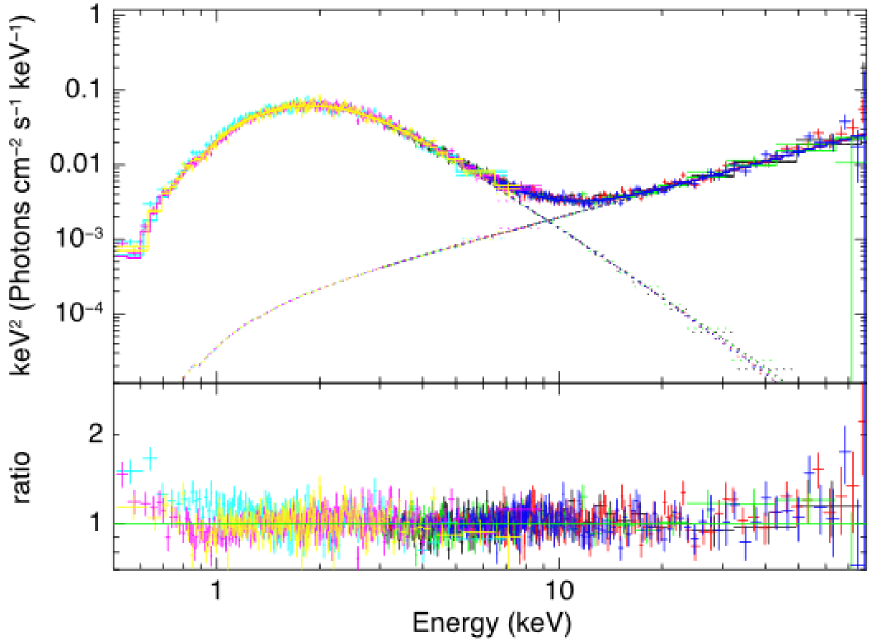

Tendulkar et al. (2015)

Bursting activity

- Short bursts
  - $\Delta t \approx 0.01 - 1$ s
  - $L_X \approx 10^{36} - 10^{41}$ erg/s

- (Intermediate) flares
  - $\Delta t \approx 1 - 10$ s
  - $L_X \approx 10^{41} - 10^{43}$ erg/s

- Giant flares
  - $\Delta t \approx 10^2$ s
  - $L_X \approx 10^{44} - 10^{47}$ erg/s

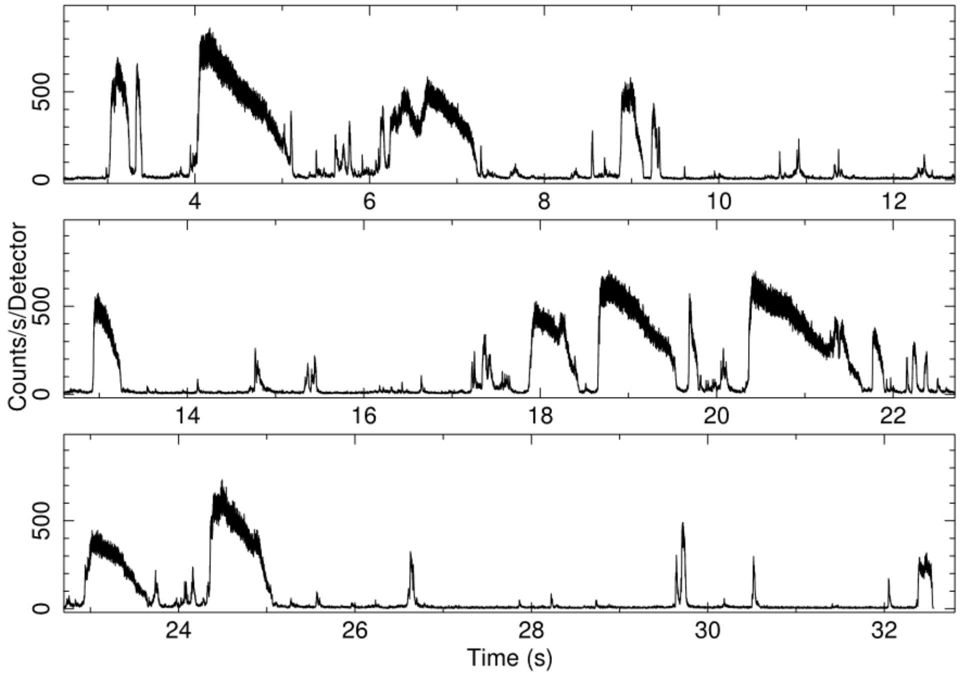

Israel et al. (2008)

Twisted-magnetosphere scenario

- The strong internal field (up to 10^{16} G) should develop a toroidal component at least of the same order

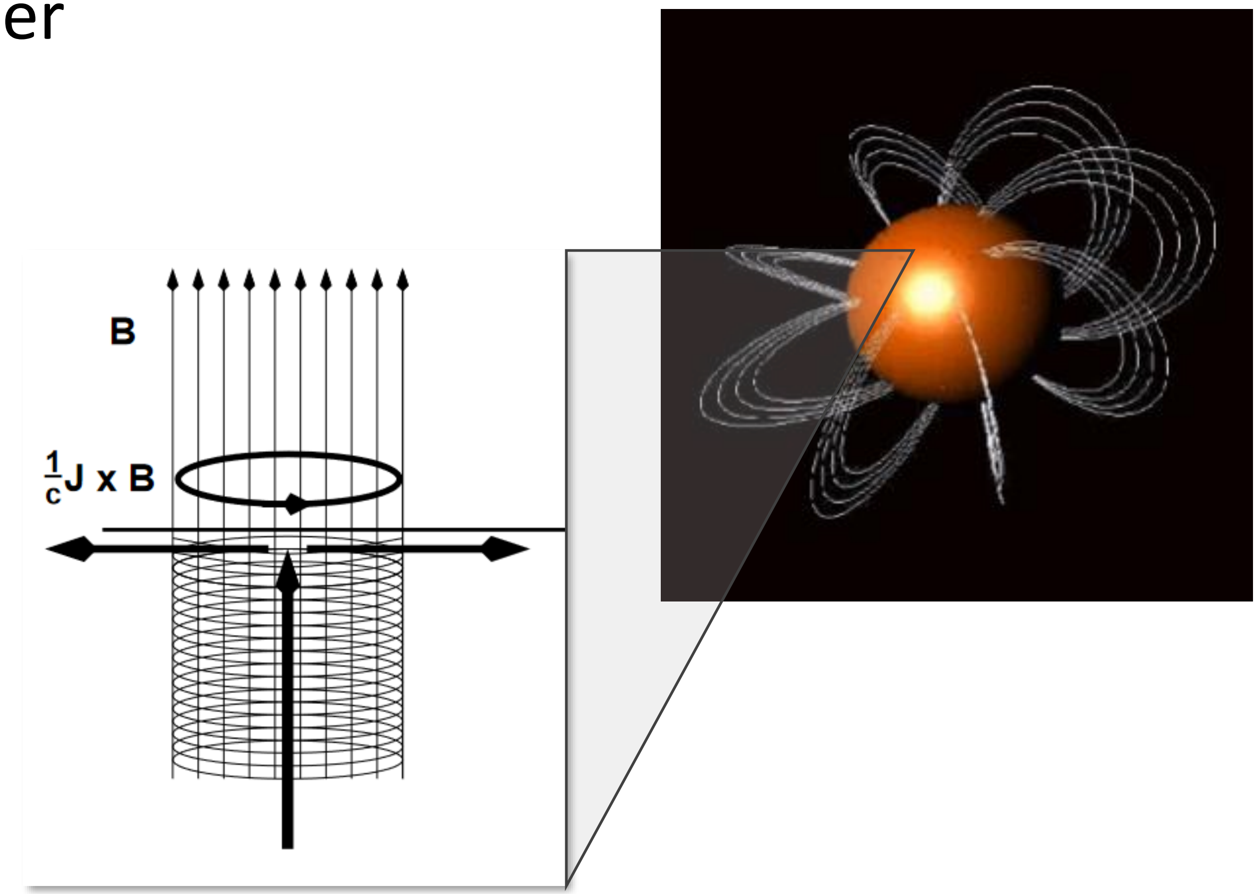

Twisted-magnetosphere scenario

- The strong internal field (up to 10^{16} G) should develop a toroidal component at least of the same order
- Once the magnetic stress exceeds the crust mechanical yield, helicity is transferred to the external field

$$\boldsymbol{B} = [B_r, B_\theta . B_\phi] = \frac{B_\mathrm{p}}{2}\left(\frac{R_\mathrm{NS}}{r}\right)^3 [2\cos\theta\,, \sin\theta\,, 0]$$

dipole

$$\boldsymbol{B} = \frac{B_\mathrm{p}}{2}\left(\frac{R_\mathrm{NS}}{r}\right)^{2+p}\left[-\frac{df}{d\cos\theta}, \frac{pf}{\sin\theta}, \sqrt{\frac{pC(p)}{p+1}}\frac{f^{1+1/p}}{\sin\theta}\right]$$

twisted dipole

$0 < p \leq 1$

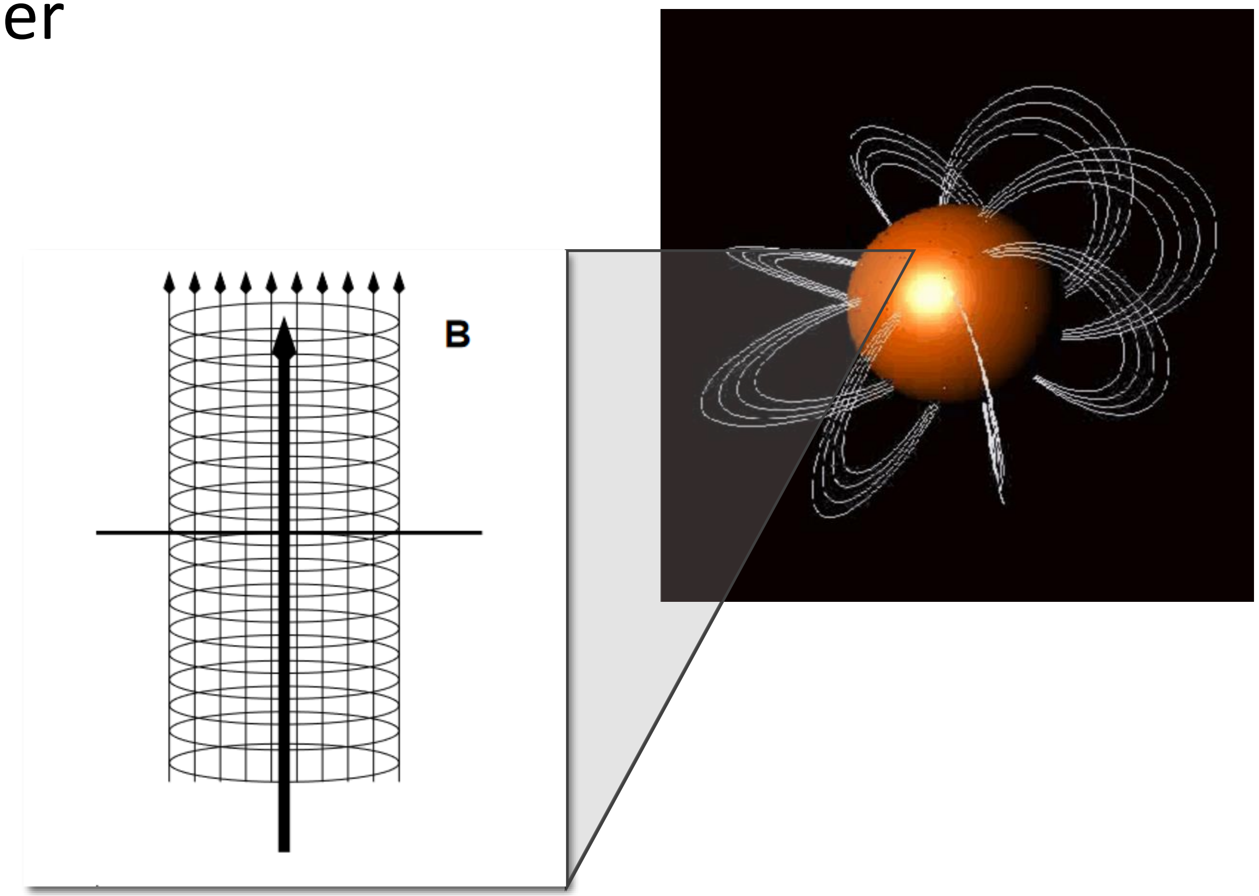

Twisted-magnetosphere scenario

$$\nabla \times \boldsymbol{B}_{\rm dip} = 4\pi \boldsymbol{j}/c$$

$\parallel$ $\Downarrow$

0 no currents

$$\nabla \times \boldsymbol{B}_{\rm twist} = 4\pi \boldsymbol{j}/c$$

$\nparallel$ $\Downarrow$

0 currents

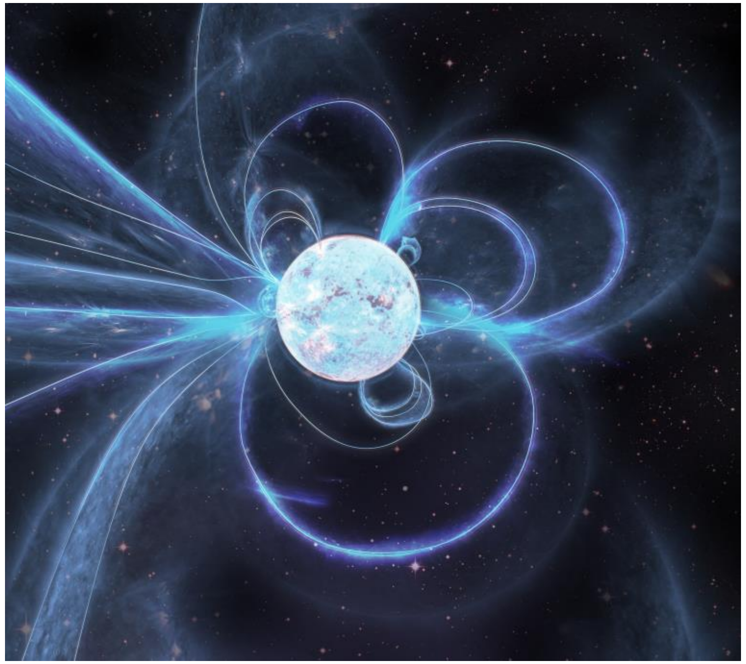

- Magnetosphere is populated by charged particles:

$$n_e \sim \frac{B}{r\beta}\left(\frac{B_\phi}{B_\theta}\right)$$

- The magnetosphere is optically thick for RCS ($\omega = \omega_{\rm cyc}$) onto <u>electrons</u>

Magnetar model achievements (till IXPE)

- RCS of thermal photons onto magnetospheric particles generates PL tails at soft X-ray energies

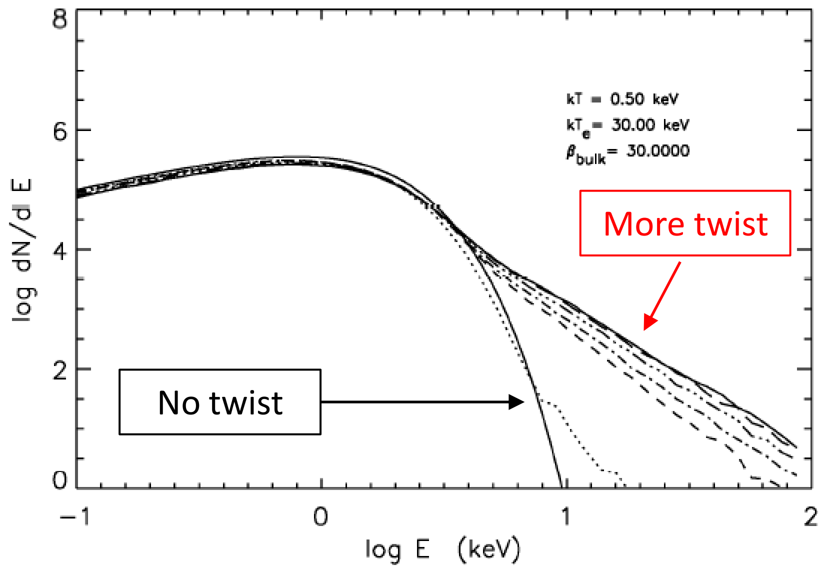

Nobili et al. (2008)

Magnetar model achievements (till IXPE)

- RCS of thermal photons onto magnetospheric particles generates PL tails at soft X-ray energies
- Internal magnetic stresses on the star crust induce injection of e^-e^+ fireballs enclosed in the magnetosphere (at the base of burst emission)
- Magnetic scattering models can explain the observed spectral properties

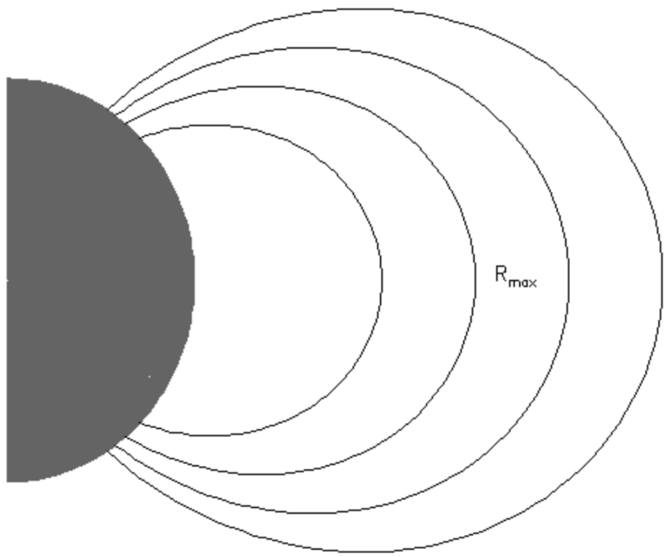

Magnetar model alternatives

- The P-$\dot{P}$ estimate of the magnetic field strength holds for:
  - dipolar fields (magnetar field topology not dipolar)
  - emission energy all supplied by rotation (need for another source of energy)

- Magnetar phenomenology very different from other NSs
  - strongly-magnetized ($\approx 10^9$ G) white dwarfs?
  - disrupting events for SGRs?

May polarimetry provide new constraints?

Polarization in strongly magnetized environments

- The polarization state of photons can be studied solving the wave equation

$$\nabla \times (\bar{\boldsymbol{\mu}} \cdot \nabla \times \boldsymbol{E}) = \frac{\omega^2}{c^2} \boldsymbol{\epsilon} \cdot \boldsymbol{E}$$

magnetic permeability tensor (inverse)

dielectric tensor

Polarization in strongly magnetized environments

- The polarization state of photons can be studied solving the wave equation

$$\nabla \times (\bar{\boldsymbol{\mu}} \cdot \nabla \times \boldsymbol{E}) = \frac{\omega^2}{c^2} \boldsymbol{\epsilon} \cdot \boldsymbol{E}$$

- $\boldsymbol{\epsilon}$ and $\bar{\boldsymbol{\mu}}$ contain all the interaction terms

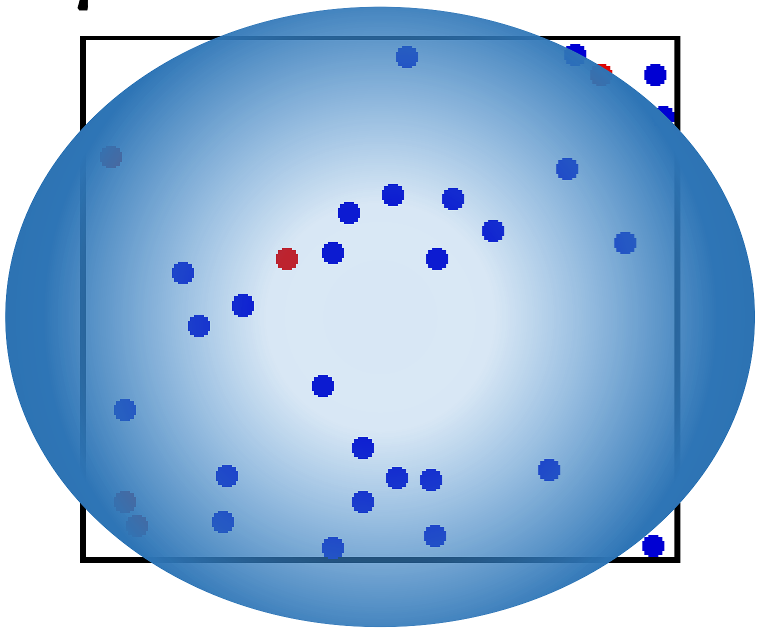

plasma

Polarization in strongly magnetized environments

- The polarization state of photons can be studied solving the wave equation

$$\nabla \times (\bar{\boldsymbol{\mu}} \cdot \nabla \times \boldsymbol{E}) = \frac{\omega^2}{c^2} \boldsymbol{\epsilon} \cdot \boldsymbol{E}$$

- $\boldsymbol{\epsilon}$ and $\bar{\boldsymbol{\mu}}$ contain all the interaction terms

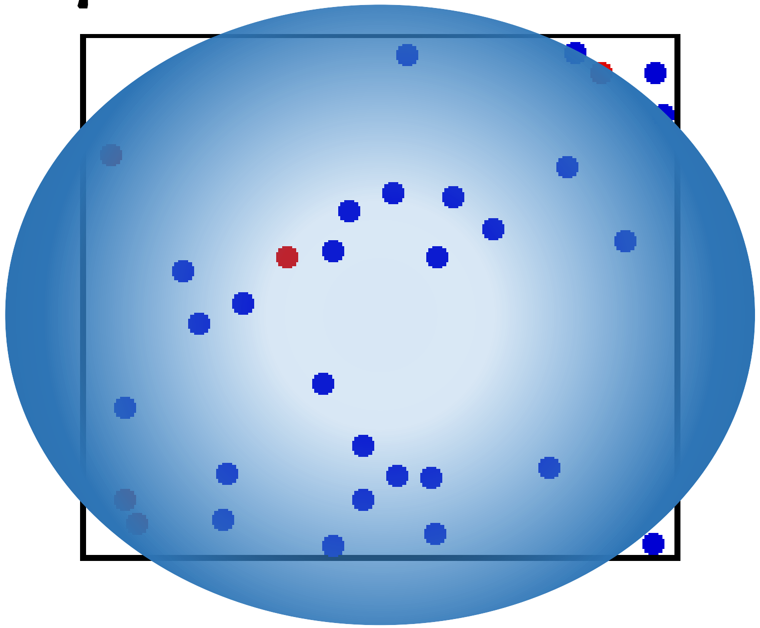

plasma

In strong $\boldsymbol{B}$ fields the charge motion is quantized

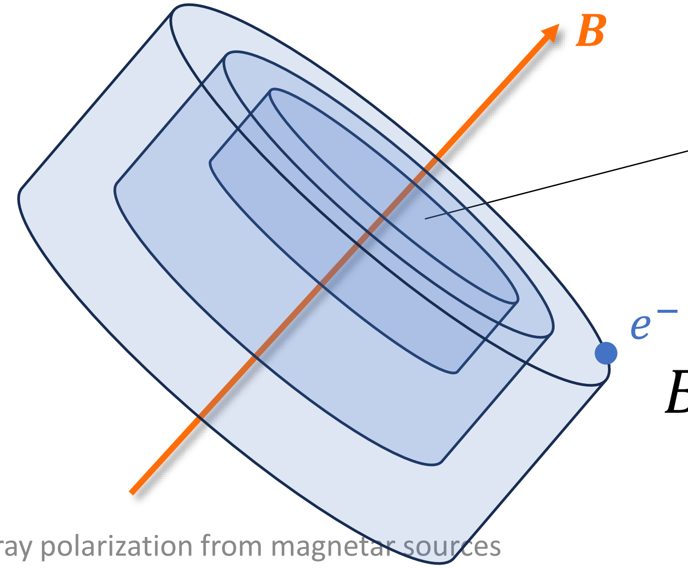

1st Landau level energy

$$\hbar\omega_{\rm B} = \frac{\hbar e B_{\rm Q}}{m_{\rm e} c} = m_e c^2$$

$$\Downarrow$$

$$B_{\rm Q} = \frac{m_e^2 c^3}{\hbar e} = 4.414 \times 10^{13}\ {\rm G}$$

Polarization in strongly magnetized environments

- The polarization state of photons can be studied solving the wave equation

$$\nabla \times (\bar{\boldsymbol{\mu}} \cdot \nabla \times \boldsymbol{E}) = \frac{\omega^2}{c^2} \boldsymbol{\epsilon} \cdot \boldsymbol{E}$$

- $\boldsymbol{\epsilon}$ and $\bar{\boldsymbol{\mu}}$ contain all the interaction terms

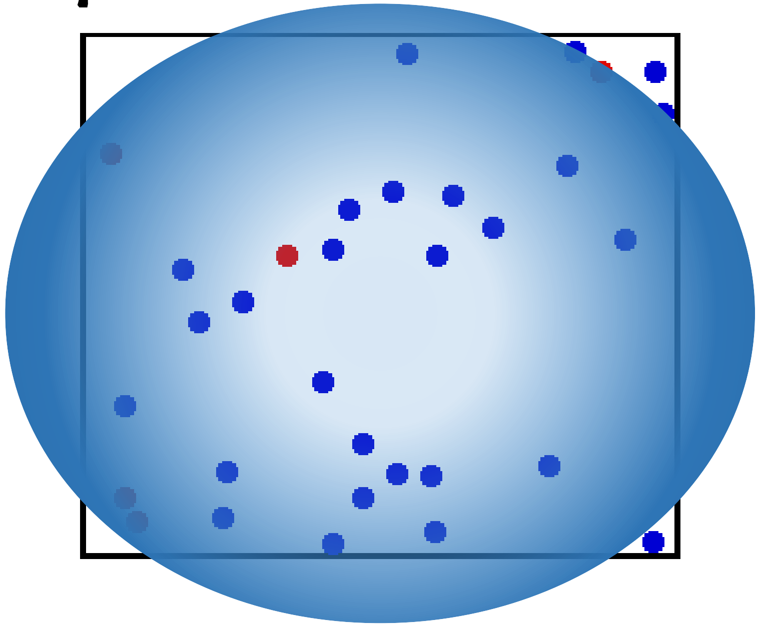

plasma

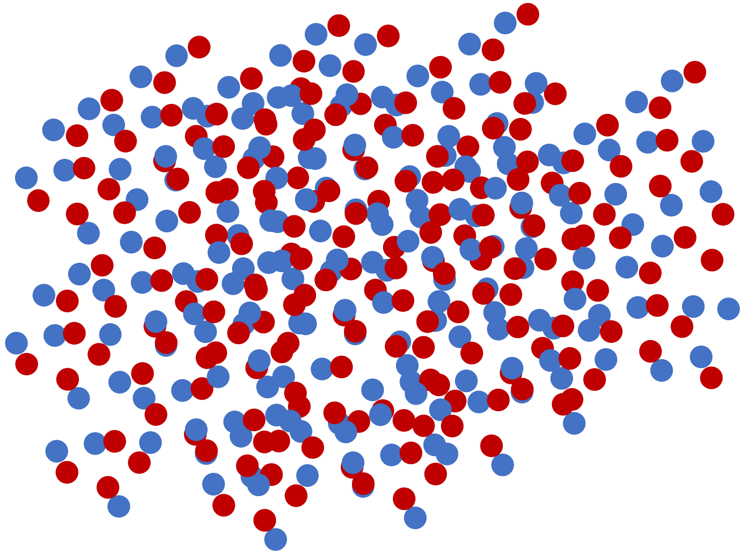

vacuum

Polarization in strongly magnetized environments

- The polarization state of photons can be studied solving the wave equation

$$\nabla \times (\bar{\boldsymbol{\mu}} \cdot \nabla \times \boldsymbol{E}) = \frac{\omega^2}{c^2} \boldsymbol{\epsilon} \cdot \boldsymbol{E}$$

- $\boldsymbol{\epsilon}$ and $\bar{\boldsymbol{\mu}}$ contain all the interaction terms

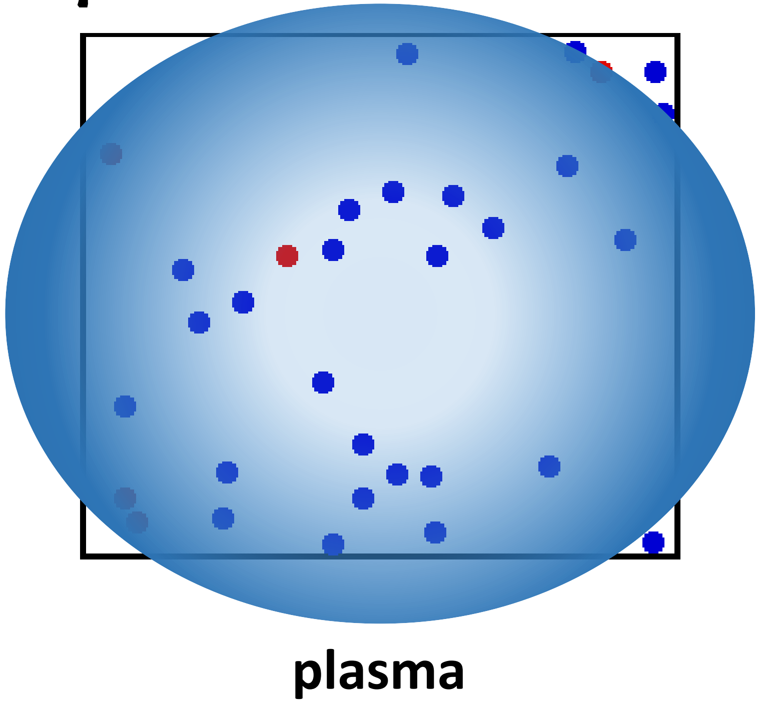

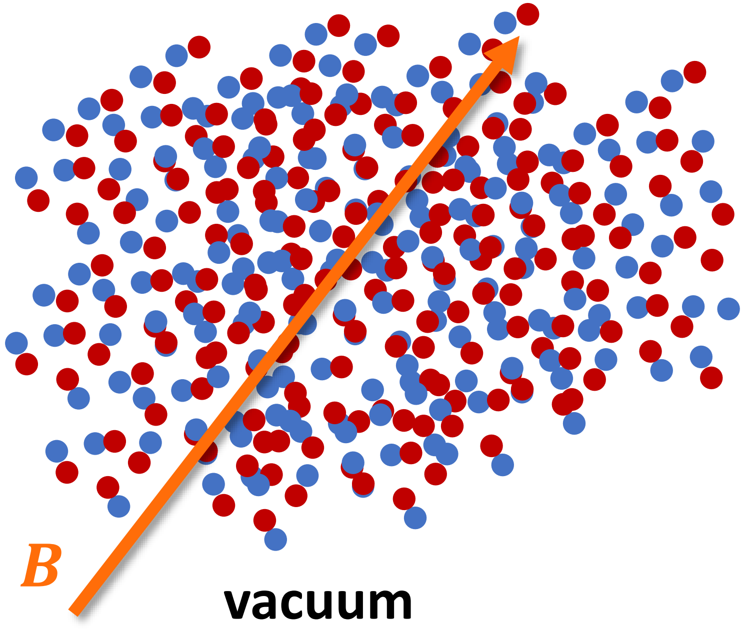

Polarization in strongly magnetized environments

- The polarization state of photons can be studied solving the wave equation

$$\nabla \times (\bar{\boldsymbol{\mu}} \cdot \nabla \times \boldsymbol{E}) = \frac{\omega^2}{c^2} \boldsymbol{\epsilon} \cdot \boldsymbol{E}$$

- $\boldsymbol{\epsilon}$ and $\bar{\boldsymbol{\mu}}$ contain all the interaction terms

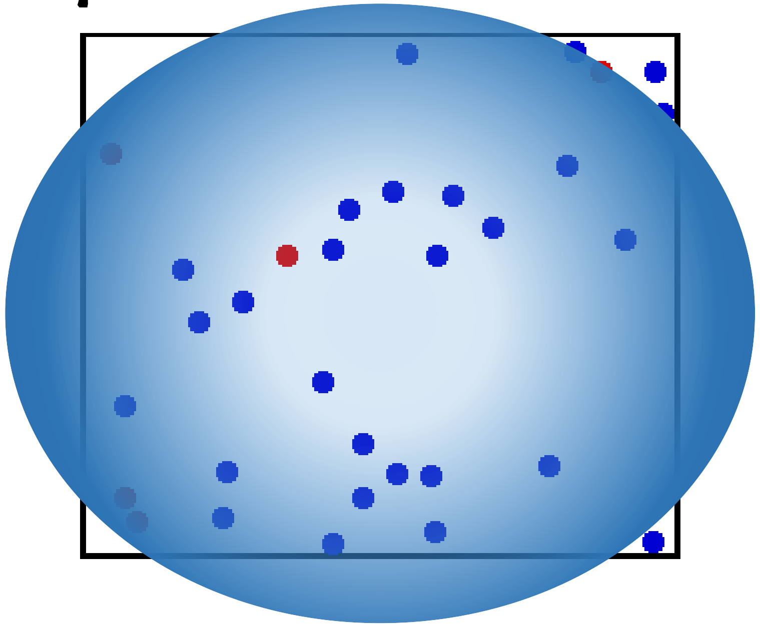

plasma

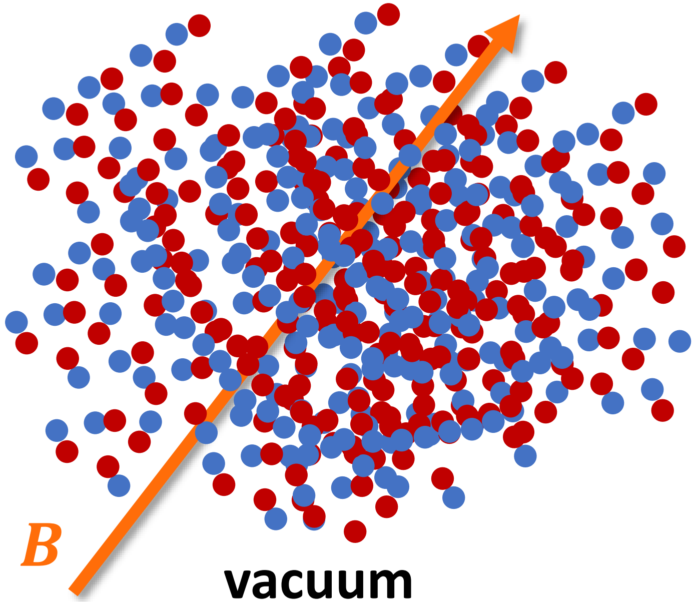

vacuum

Normal modes of polarization

- Where plasma or vacuum terms dominate in the dielectric tensor radiation is approximately linearly polarized

$$\hat{\boldsymbol{E}} \approx \begin{pmatrix} 1 \\ 0 \\ 0 \end{pmatrix} \quad \text{or} \quad \begin{pmatrix} 0 \\ 1 \\ 0 \end{pmatrix}$$

Ordinary mode **Extraordinary mode**

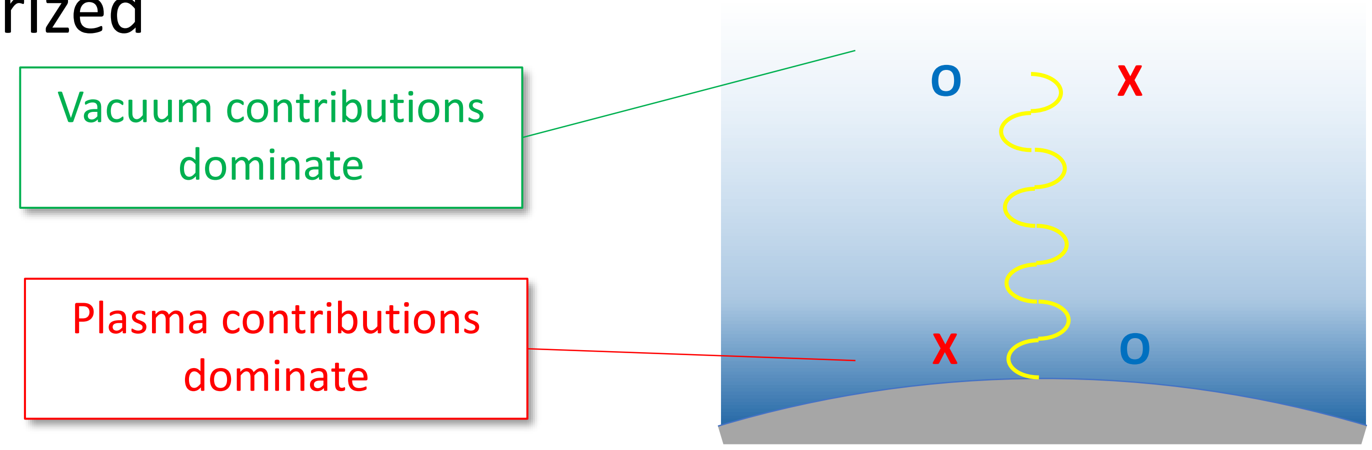

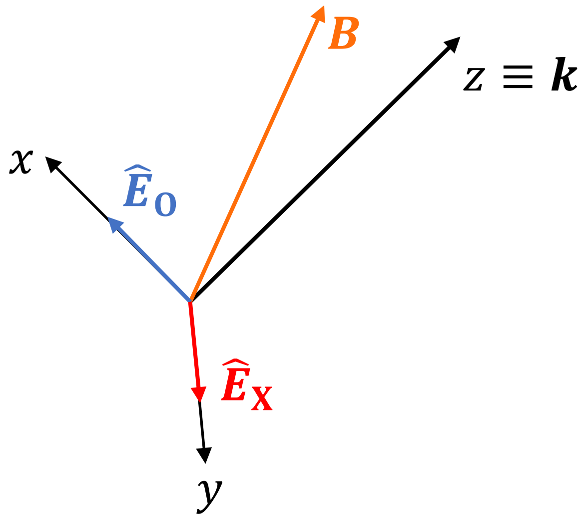

Normal modes of polarization

- Where plasma or vacuum terms dominate in the dielectric tensor radiation is approximately linearly polarized
- Something happens when plasma and vacuum contributions balance

$$\Rightarrow \quad \hat{\boldsymbol{E}} \approx \begin{pmatrix} 1 \\ 1 \\ 0 \end{pmatrix}$$ **Circularly polarized**

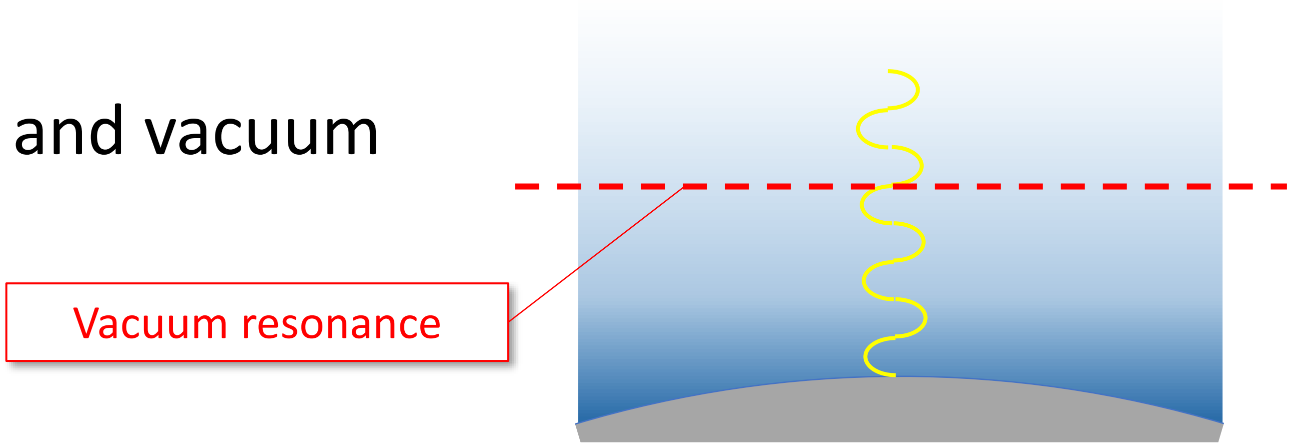

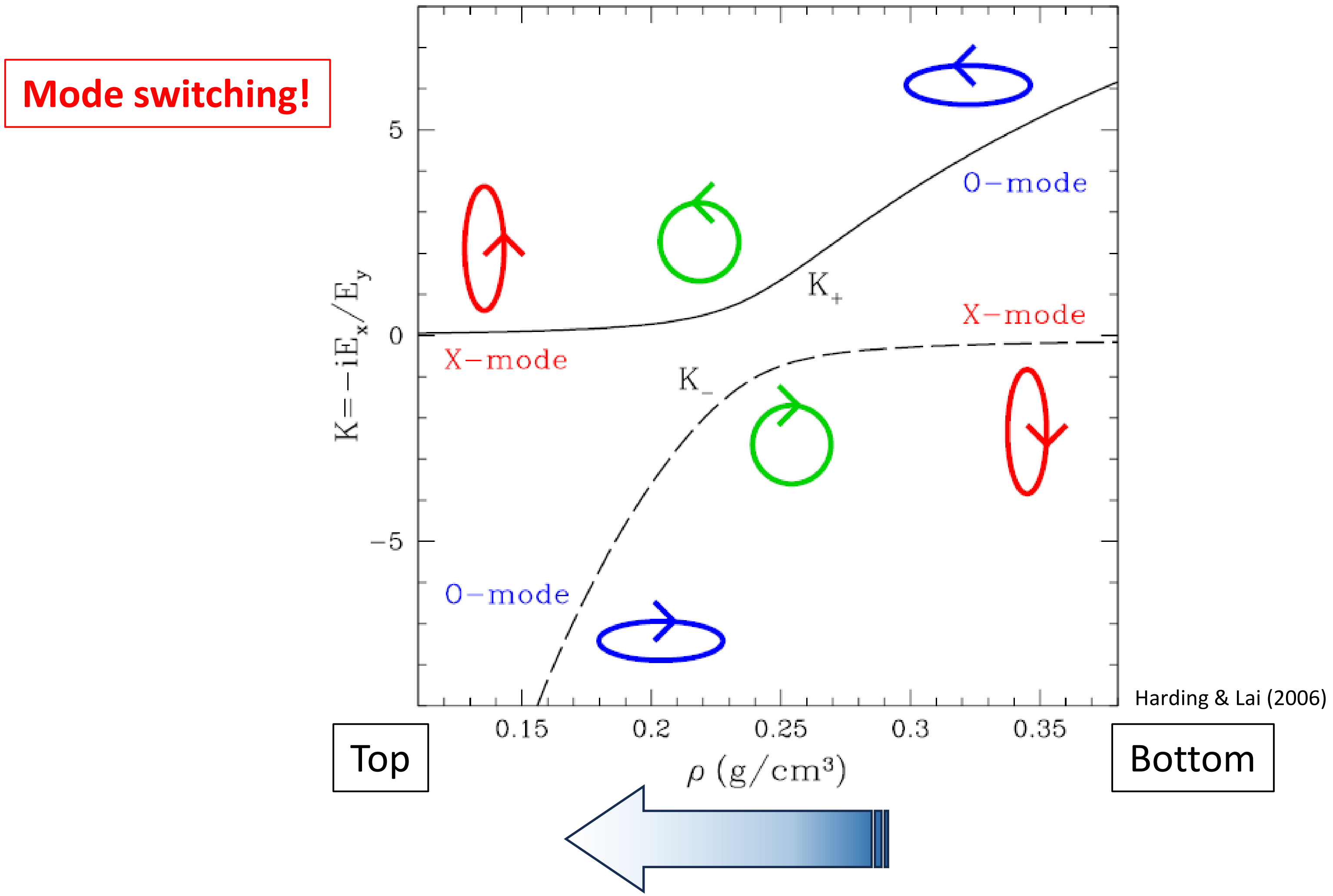

Mode switching!
5
0
−5
K=−iE_x/E_y
O−mode
K_+
X−mode
X−mode
K_−
O−mode
0.15
0.2
0.25
0.3
0.35
ρ (g/cm³)
Top
Bottom
Harding & Lai (2006)

Dichroism in strongly-magnetized plasma

- In strong fields ($B \gtrsim B_{\mathrm{Q}}$) and $E \ll \hbar\omega_B$ plasma is (generally) transparent for X-mode photons

$$\sigma_{\mathrm{OO}} \sim \sigma_{\mathrm{unmag}}$$

$$\sigma_{\mathrm{OX}} \sim \left(\frac{B}{B_{\mathrm{Q}}}\right)^{-2} \sigma_{\mathrm{OO}}$$

$$\sigma_{\mathrm{XO}} \sim \left(\frac{B}{B_Q}\right)^{-2} \sigma_{\mathrm{OO}}$$

$$\sigma_{\mathrm{XX}} \sim \left(\frac{B}{B_Q}\right)^{-2} \sigma_{\mathrm{OO}}$$

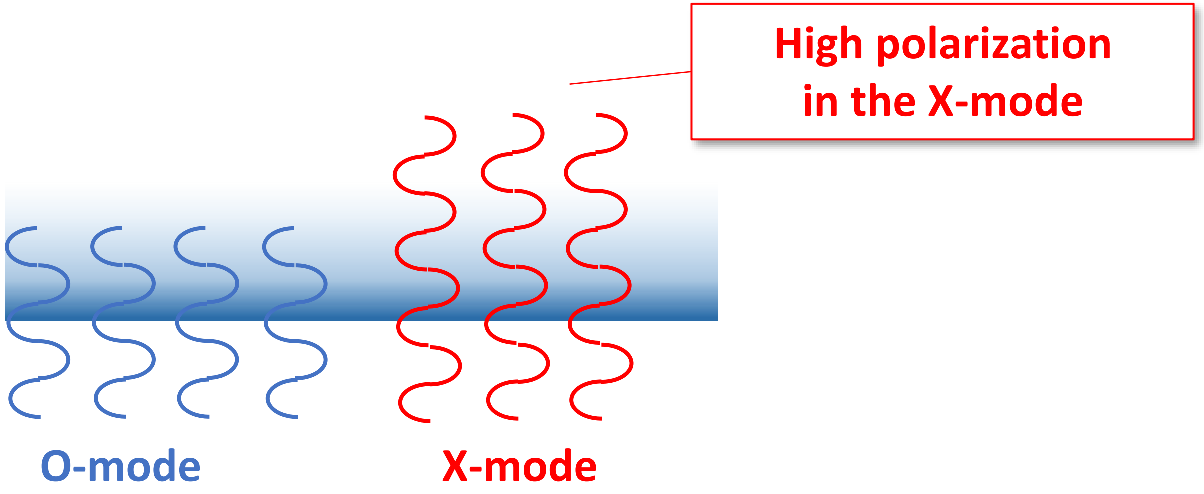

Dichroism in strongly-magnetized plasma

- In strong fields ($B \gtrsim B_{\mathrm{Q}}$) and $E \ll \hbar\omega_B$ plasma is (generally) transparent for X-mode photons
- Things are different at the cyclotron resonance ($\omega = \omega_{\mathrm{B}}$)

$$\sigma_{\mathrm{OO}} = \frac{1}{3}\sigma_{\mathrm{OX}} \qquad \sigma_{\mathrm{XX}} = 3\sigma_{\mathrm{XO}}$$

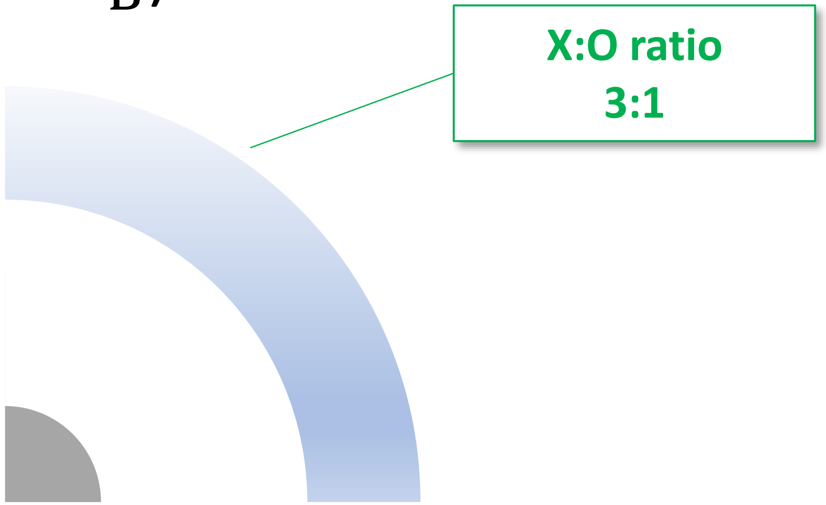

Polarization transport in the magnetized vacuum

- Solving the wave equation accounting for vacuum effects only it reduces to

$$\frac{2}{k_0\delta(B)}\frac{dE_x}{dz} = i[ME_x + PE_y] \qquad \frac{2}{k_0\delta(B)}\frac{dE_y}{dz} = i[PE_x + NE_y]$$

Polarization transport in the magnetized vacuum

- Solving the wave equation accounting for vacuum effects only it reduces to

$$\frac{2}{k_0\delta(B)}\frac{dE_x}{dz} = i[ME_x + PE_y] \qquad \frac{2}{k_0\delta(B)}\frac{dE_y}{dz} = i[PE_x + NE_y]$$

E-field evolution length:

$$\ell_{\mathrm{E}} = \frac{2}{k_0\delta} \approx 130\left(\frac{B}{10^{11}\ \mathrm{G}}\right)^{-2}\left(\frac{\hbar\omega}{1\ \mathrm{keV}}\right)^{-1}\ \mathrm{cm}$$

(Dipolar) B-field evolution length:

$$\ell_{\mathrm{B}} = \frac{B}{|\boldsymbol{k}\cdot\boldsymbol{\nabla}B|} \approx \frac{r}{3}$$

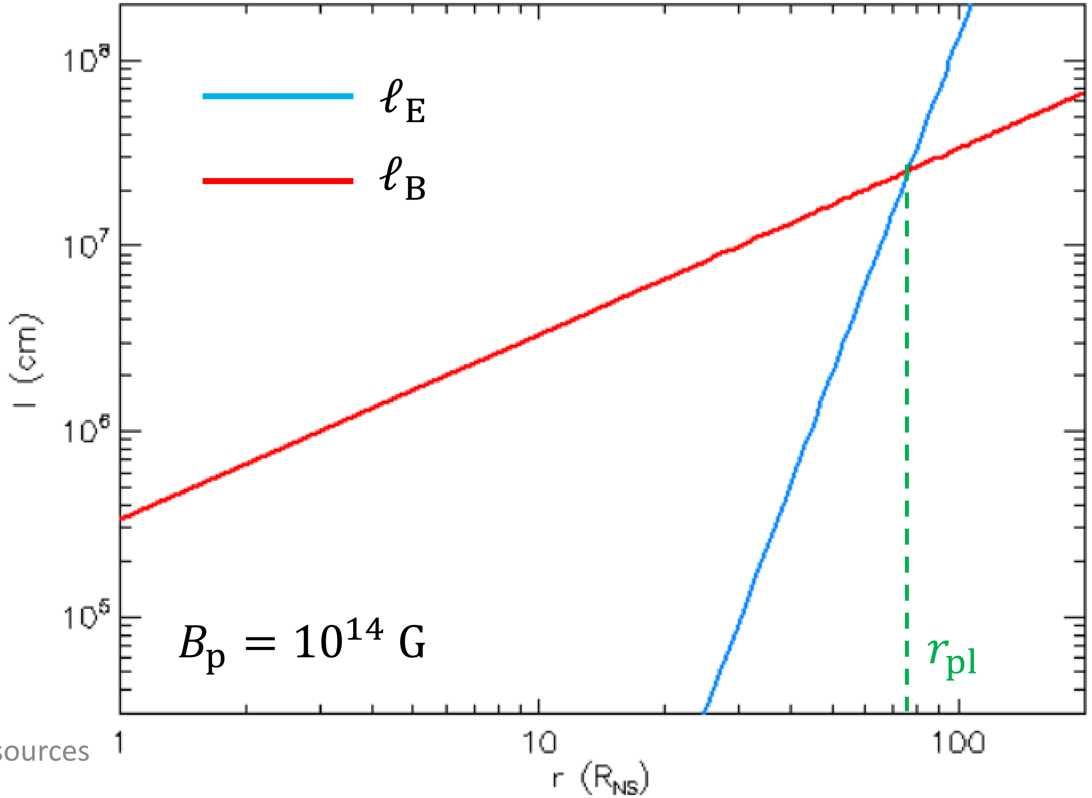

Polarization transport in the magnetized vacuum

- Solving the wave equation accounting for vacuum effects only it reduces to

$$\frac{2}{k_0\delta(B)}\frac{dE_x}{dz} = i\left[ME_x + PE_y\right] \qquad \frac{2}{k_0\delta(B)}\frac{dE_y}{dz} = i\left[PE_x + NE_y\right]$$

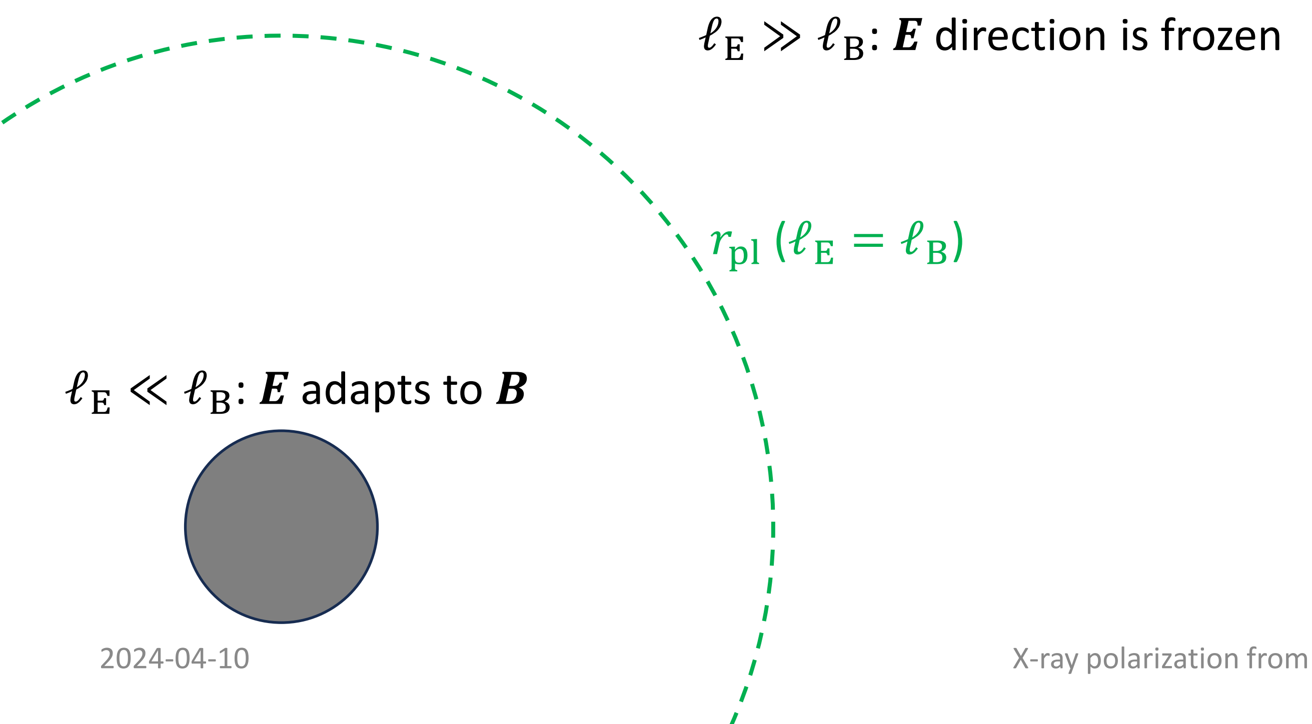

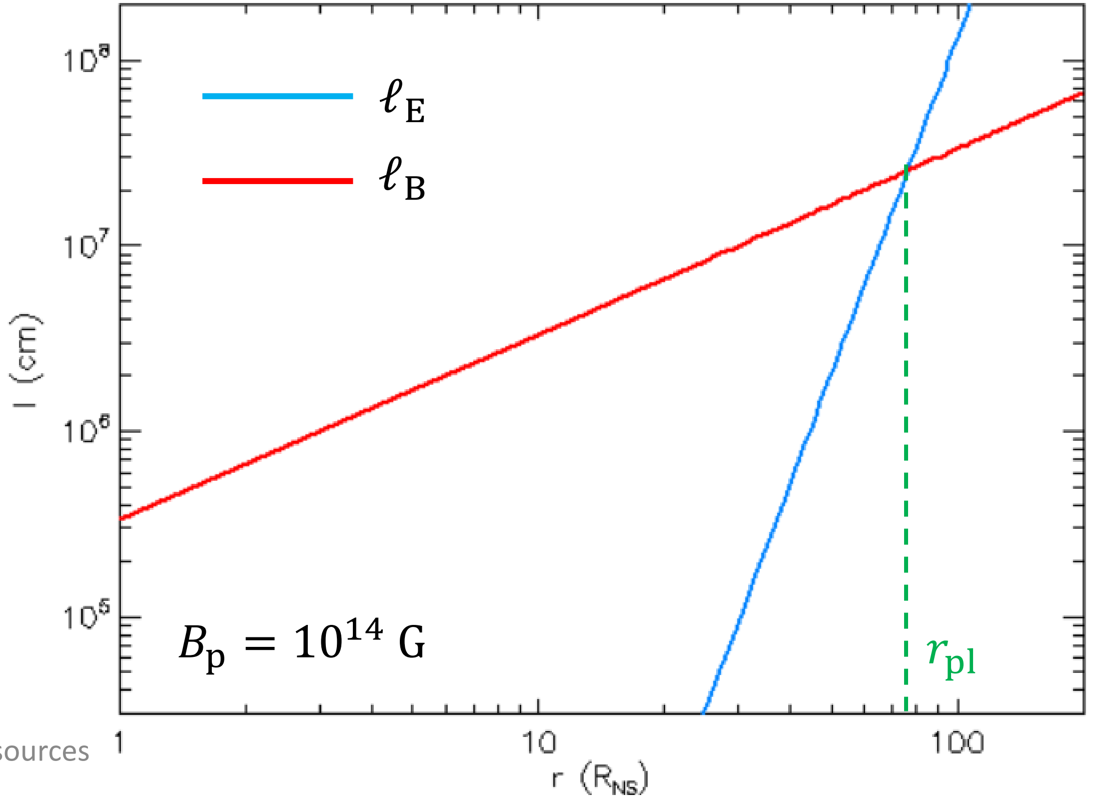

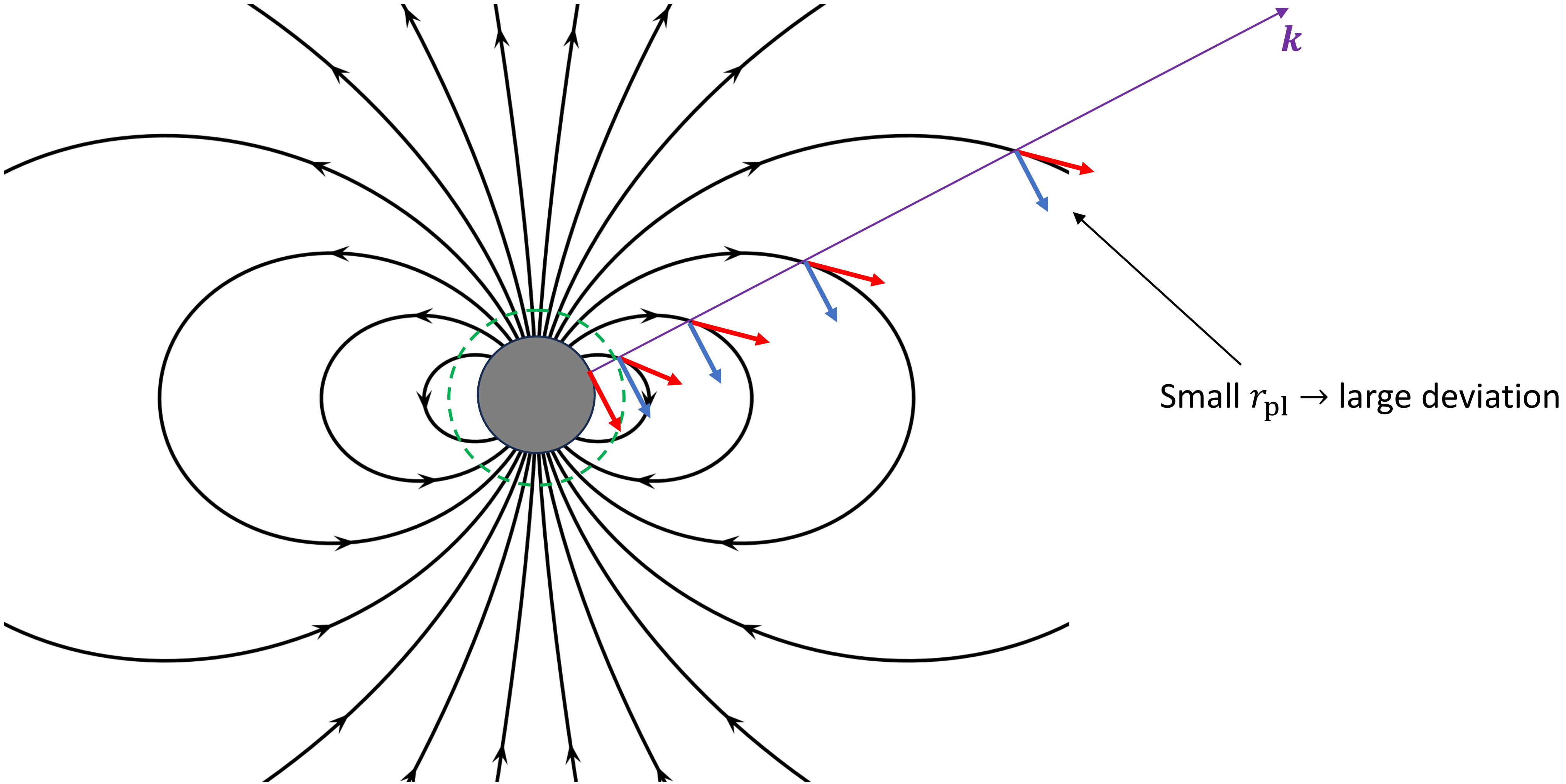
k
Small $r_{\rm pl}$ → large deviation

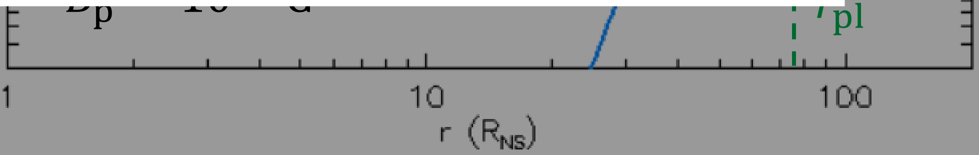
1
10
100
r (R_{NS})

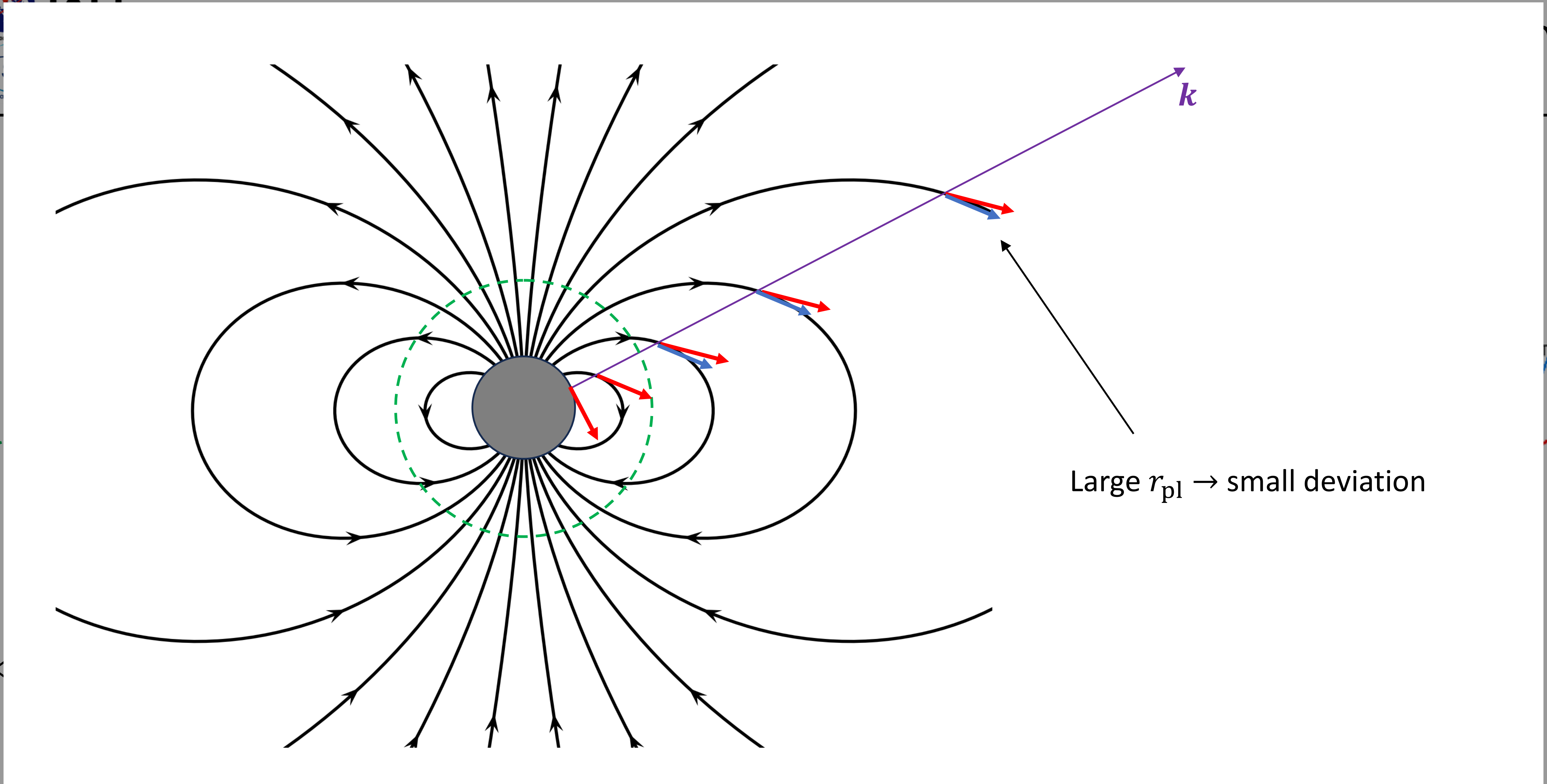

$\ell_E <$

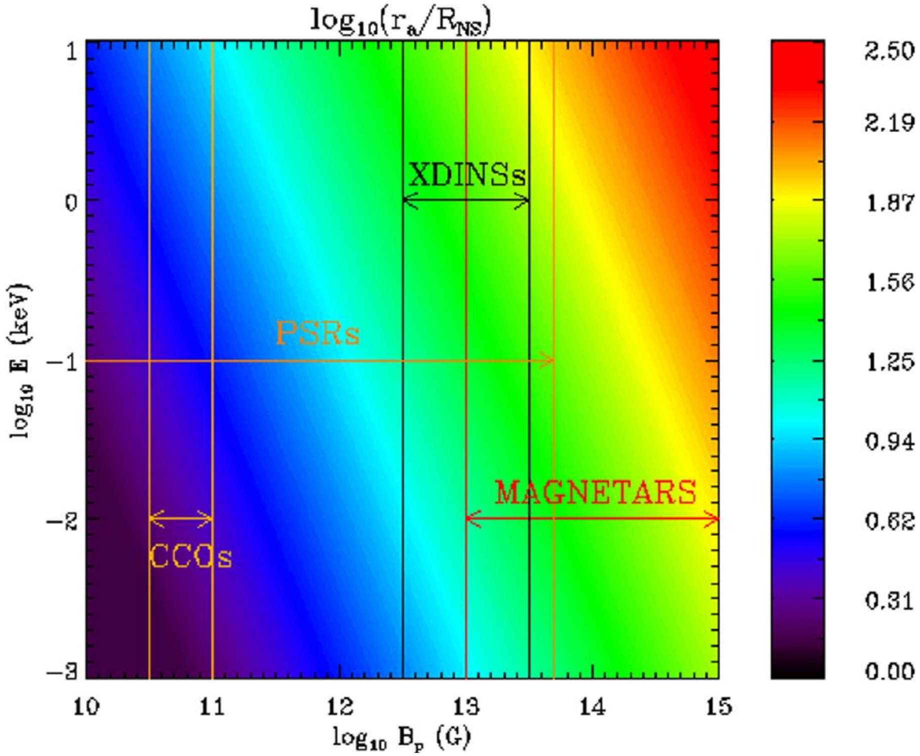

Taverna et al. (2015)

Magnetars (with the strongest $\boldsymbol{B}$) have the largest $r_{\rm pl}$

⇓

Best candidates to observe polarization of surface emission (potentially very high)

$\ell_{\rm E} <$

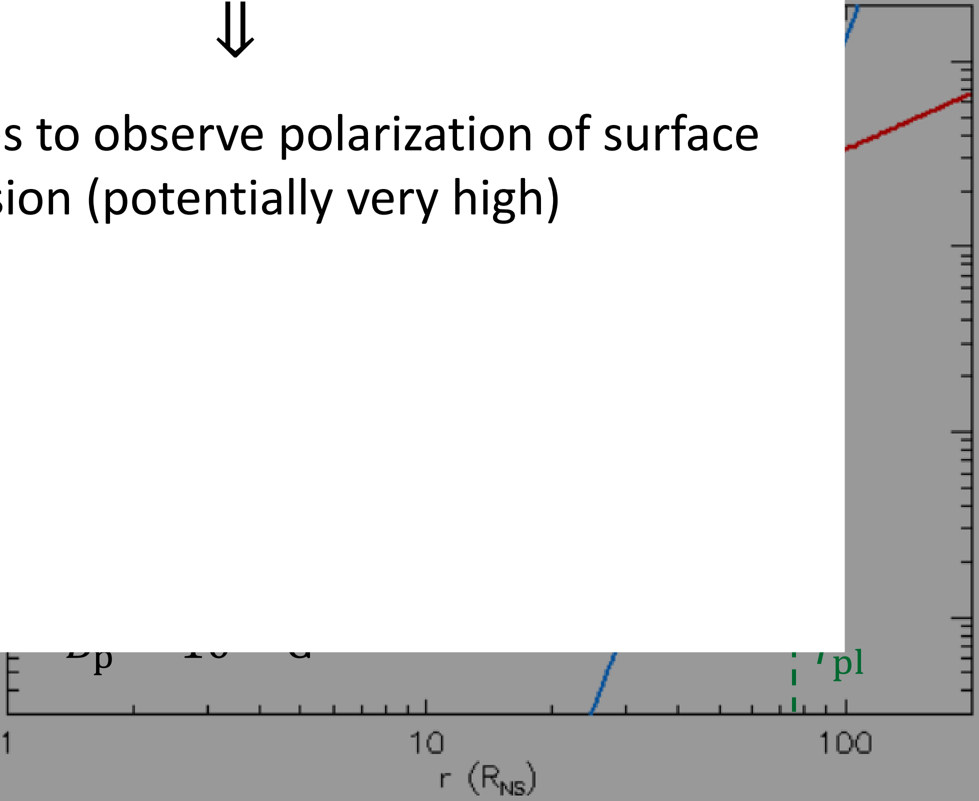

Surface emission models

- Surface photons reprocessed by a standard, magnetized atmosphere → high PD (X-mode)

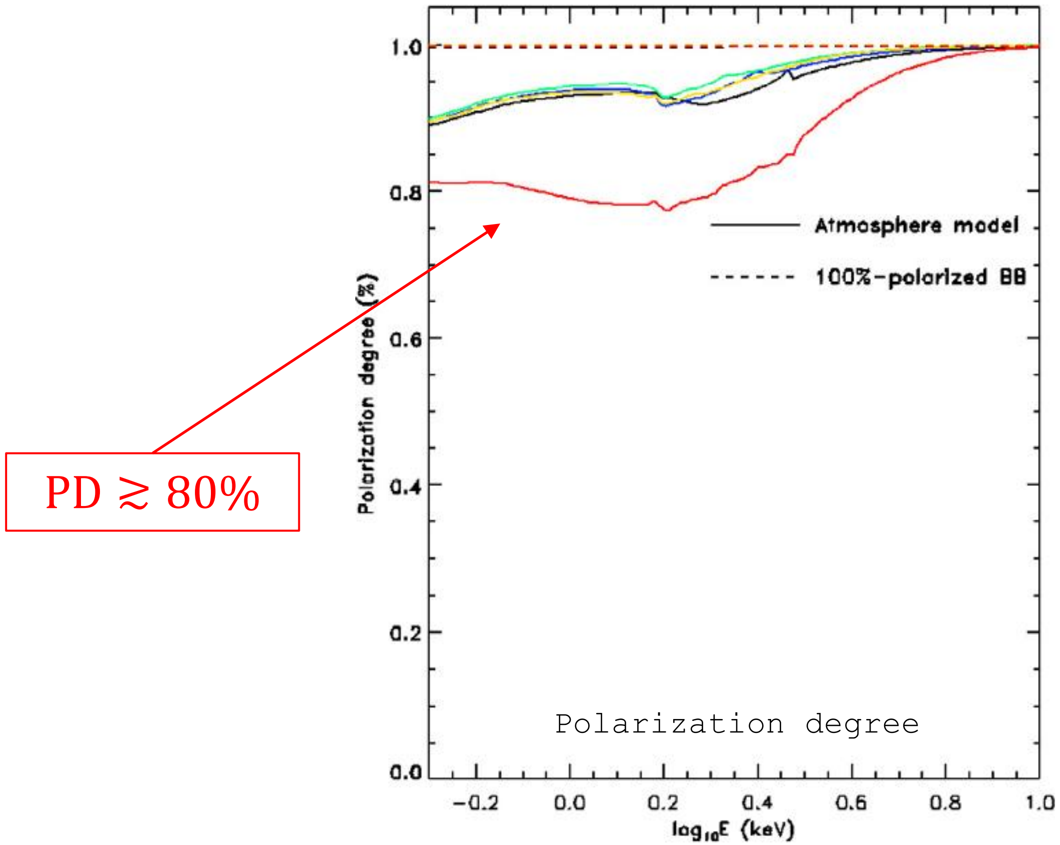

Taverna et al. (2020)

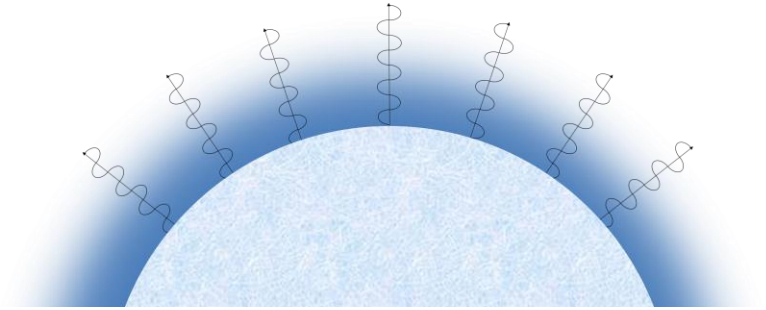

Surface emission models

- Surface photons reprocessed by a standard, magnetized atmosphere → high PD (X-mode)
- Very strong B-fields elongate atoms along the field direction → molecular chains are formed for sufficiently low T

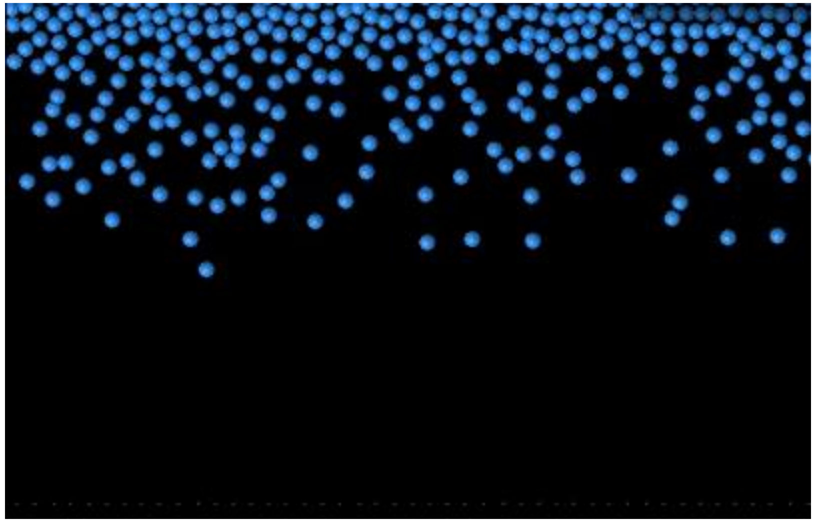

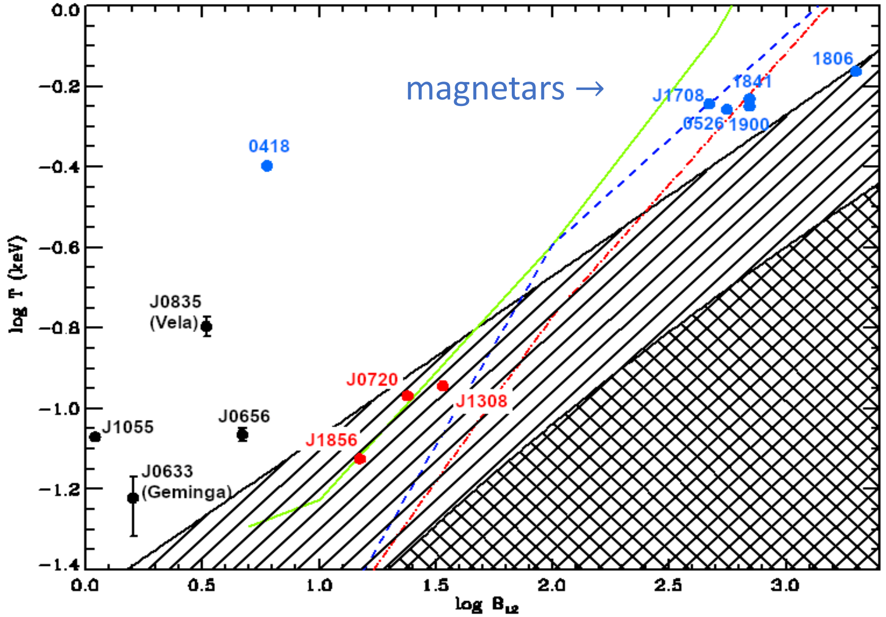

Taverna & Turolla (2024)

Surface emission models

- Surface photons reprocessed by a standard, magnetized atmosphere → high PD (X-mode)
- Very strong B-fields elongate atoms along the field direction → molecular chains are formed for sufficiently low T
- The atmosphere settles onto the surface and the (condensed) crust is left exposed
- Much lower PD (both O- and X-)

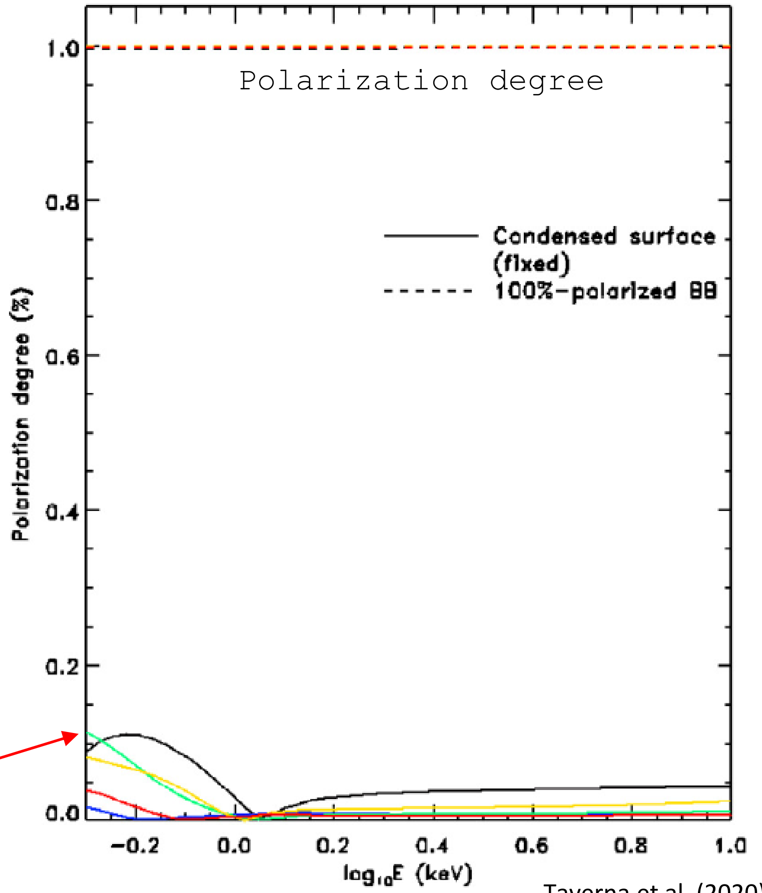

Taverna et al. (2020)

$\mathrm{PD} \lesssim 20\%$

Expected polarization degree and angle

- Different behaviors of PA with energy are expected for particular emission models and geometries

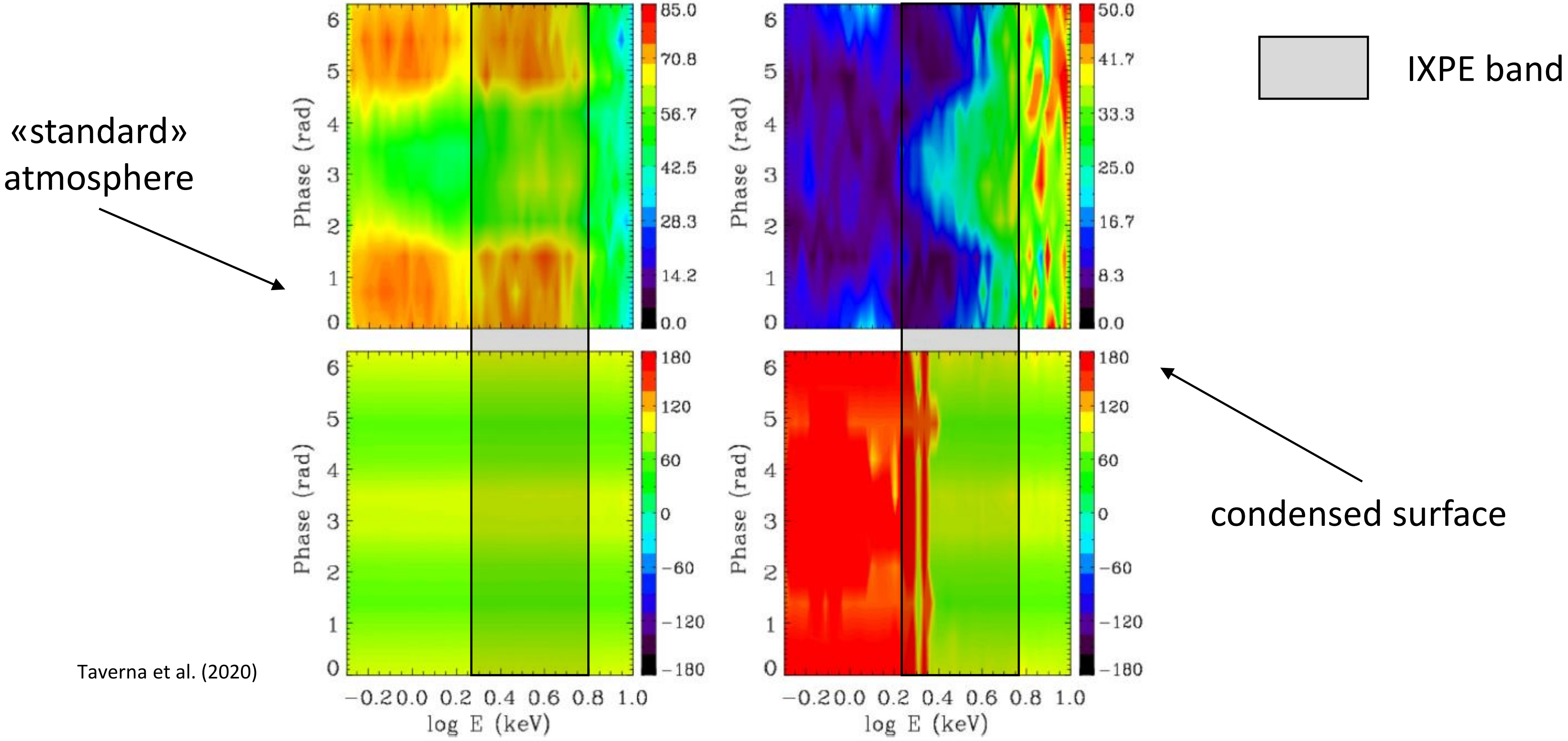

Taverna et al. (2020)

Rotating vector model (RVM)

- Variation of the polarization angle with rotational phase

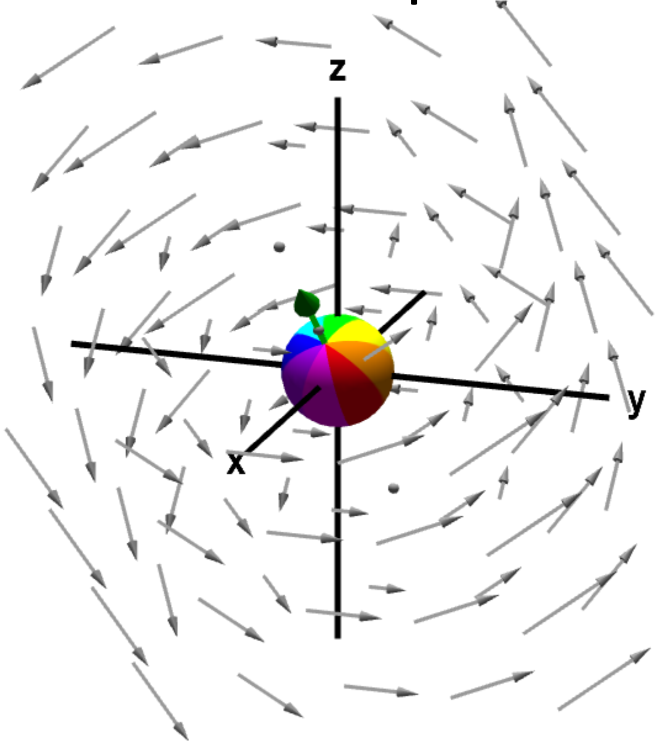

$$\tan(\mathrm{PA}) = \frac{\sin\xi \sin\phi}{\cos\chi \sin\xi \cos\phi - \sin\chi \cos\xi}$$

- Emission from small caps (e.g. in radio pulsars or in accreting X-ray pulsars)

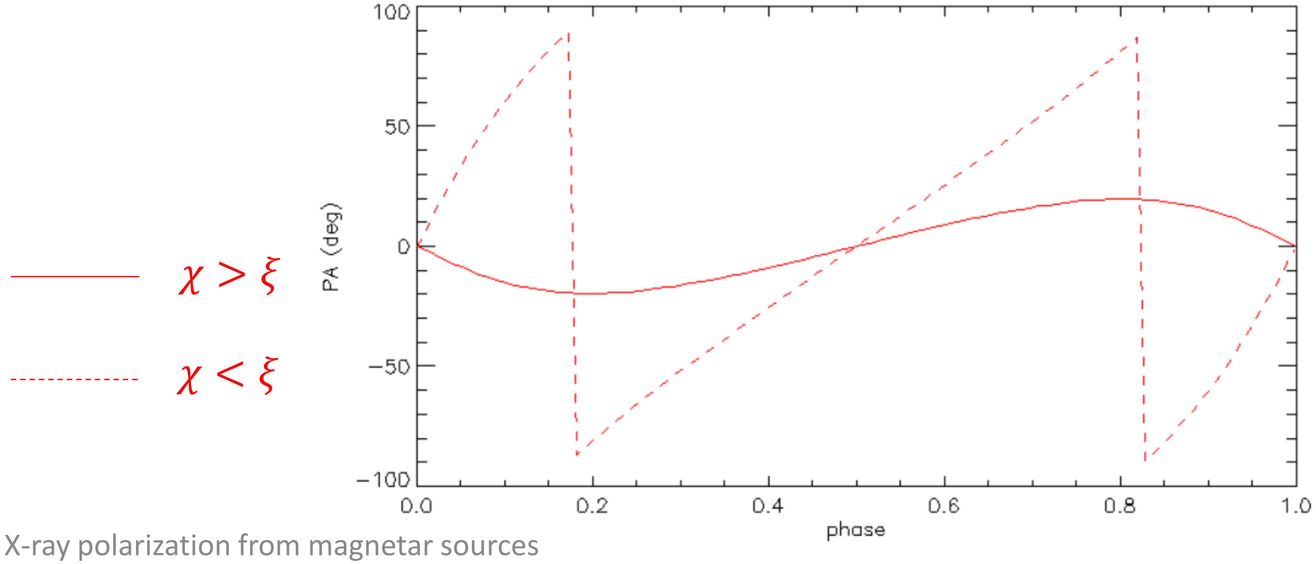

Imaging X-ray Polarimetry Explorer (IXPE)

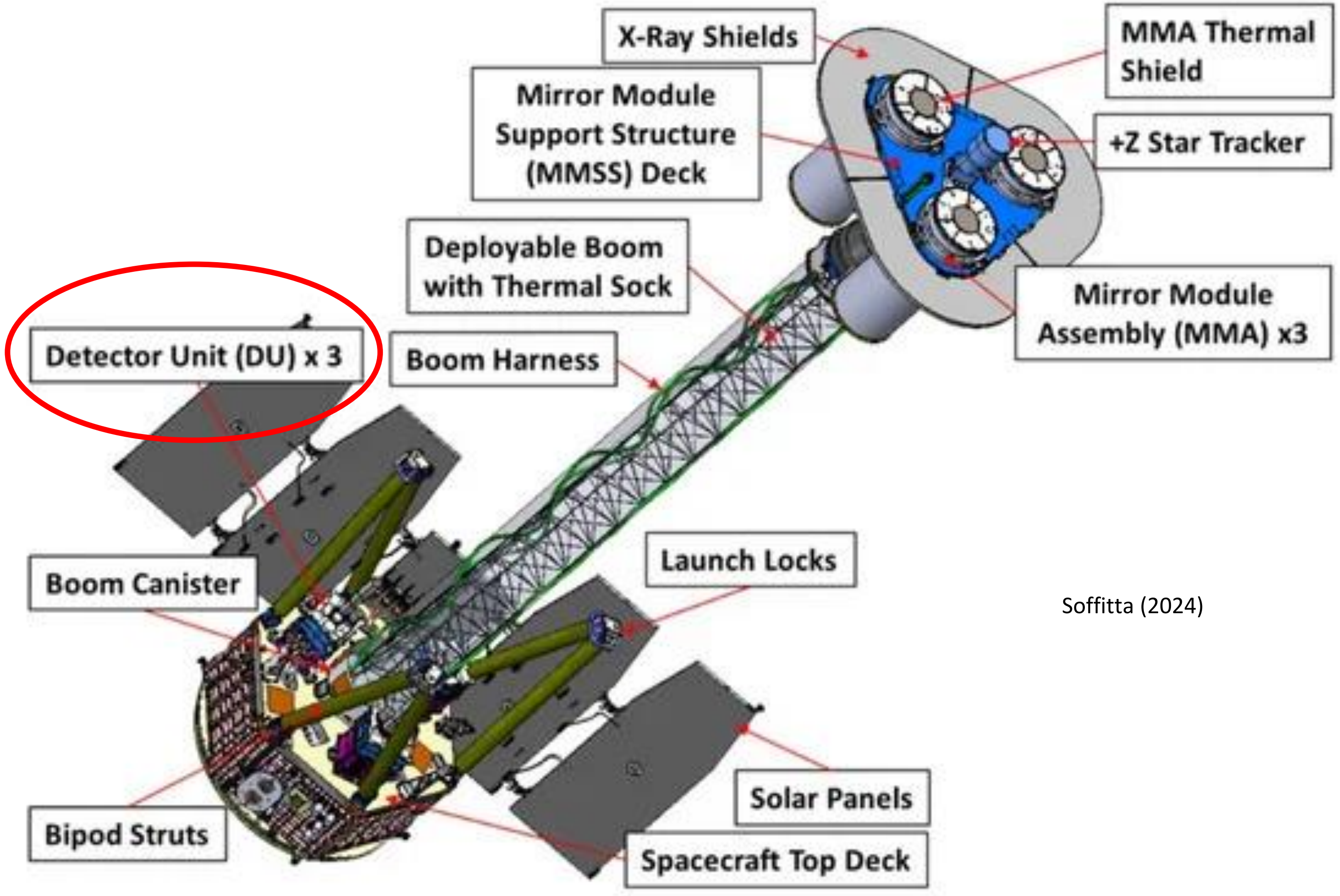

Soffitta (2024)

Imaging X-ray Polarimetry Explorer (IXPE)

- Gas Pixel Detector (GPD)

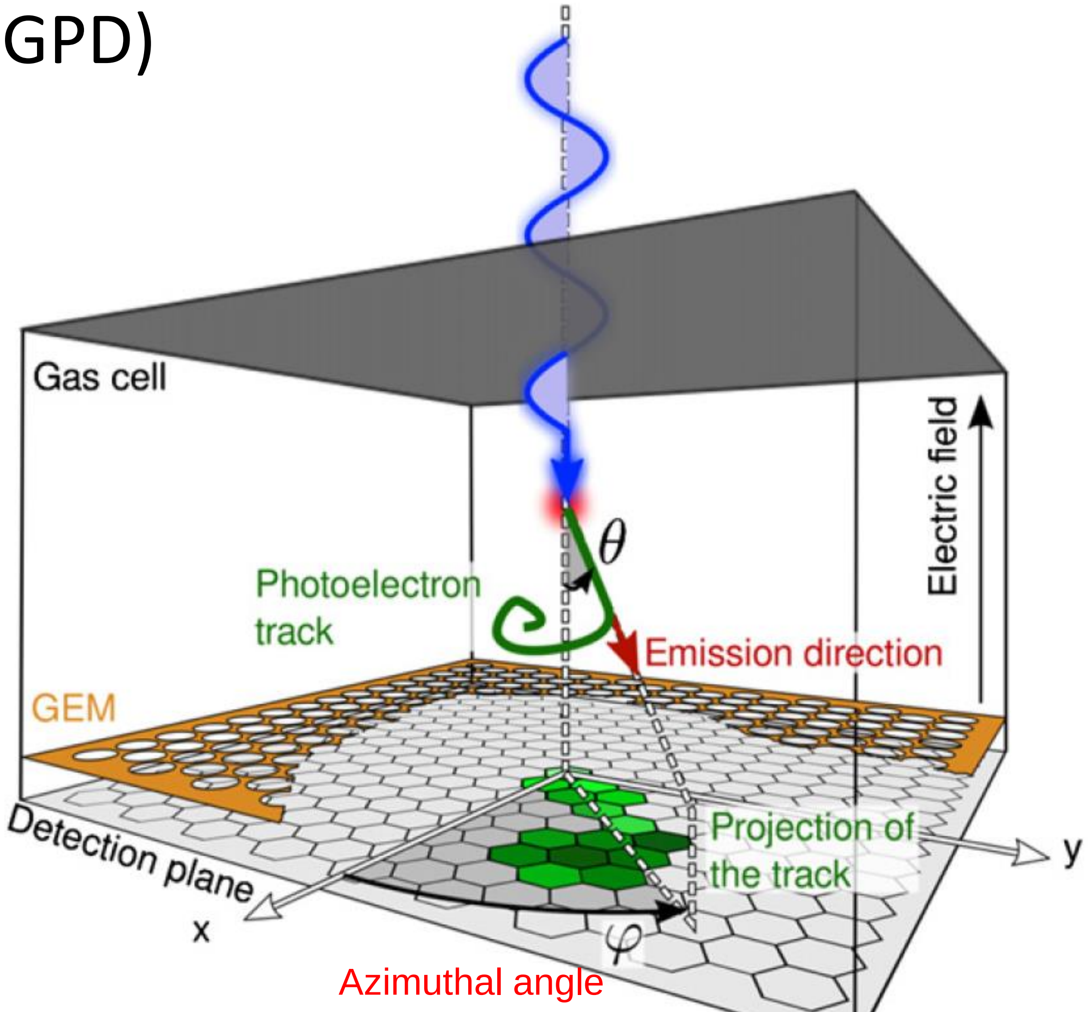

Muleri (2014)

Imaging X-ray Polarimetry Explorer (IXPE)

- Gas Pixel Detector (GPD)
- Photoelectric cross section

$$\frac{d\sigma_{\mathrm{Ph}}}{d\Omega} = r_0^2 \alpha^4 Z^5 \left(\frac{m_e c^2}{E}\right)^{\frac{7}{2}} \frac{4\sqrt{2}\sin^2\theta}{(1-\beta\cos\theta)^4}\cos^2\phi$$

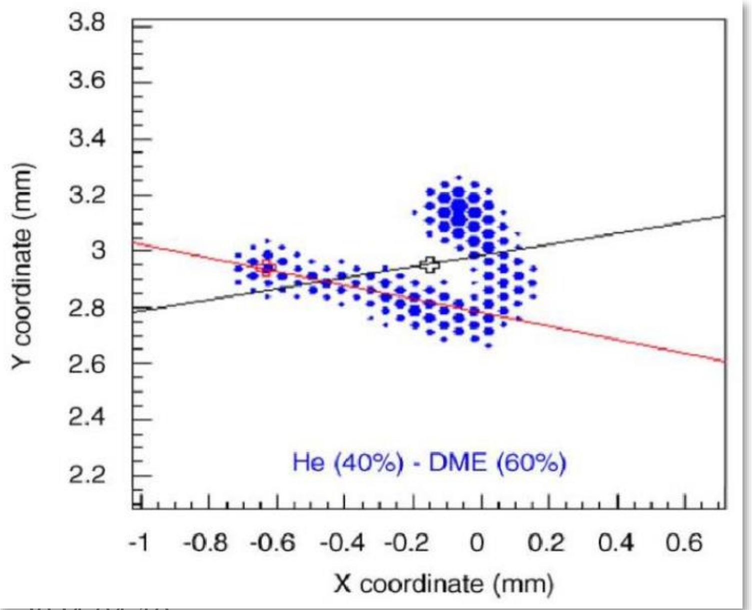

Photoelectrons most probably emitted in the direction of $\boldsymbol{E}$

Imaging X-ray Polarimetry Explorer (IXPE)

- Gas Pixel Detector (GPD)
- Photoelectric cross section
- Modulation curve

$$\mathcal{M}(\varphi) = K + A\cos^2(\varphi - \varphi_0)$$

Modulation factor μ: Amplitude for 100% polarized radiation

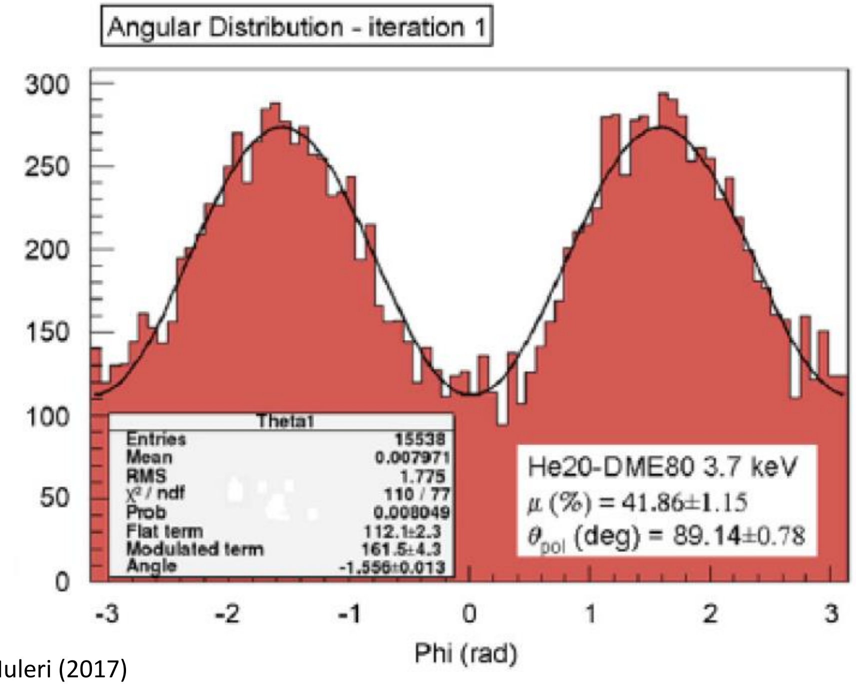

Muleri (2017)

Imaging X-ray Polarimetry Explorer (IXPE)

- Gas Pixel Detector (GPD)
- Photoelectric cross section
- Modulation curve
- Minimum Detectable Polarization

$$MDP_{99} = \frac{4.29}{\eta \mu \mathcal{S}} \sqrt{\frac{\mathcal{B} + \eta \mathcal{S}}{\mathcal{A} t_{\text{exp}}}}$$

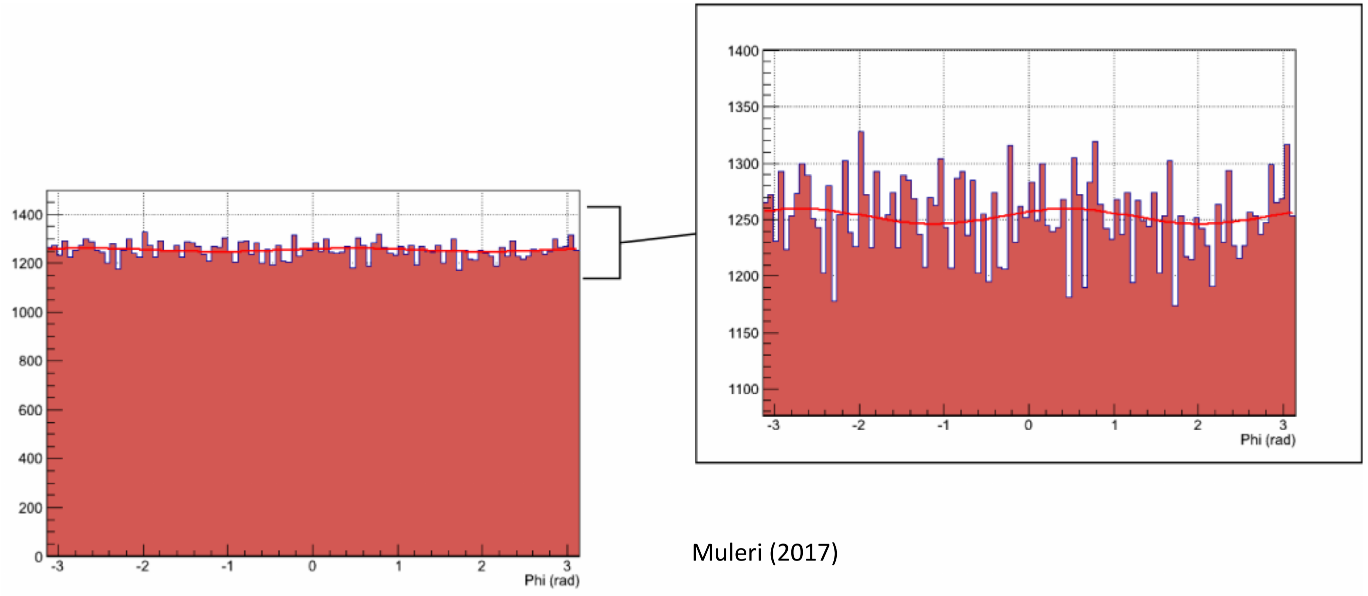

Muleri (2017)

Imaging X-ray Polarimetry Explorer (IXPE)

- Gas Pixel Detector (GPD)
- Photoelectric cross section
- Modulation curve
- Minimum Detectable Polarization
- Polarization measurement

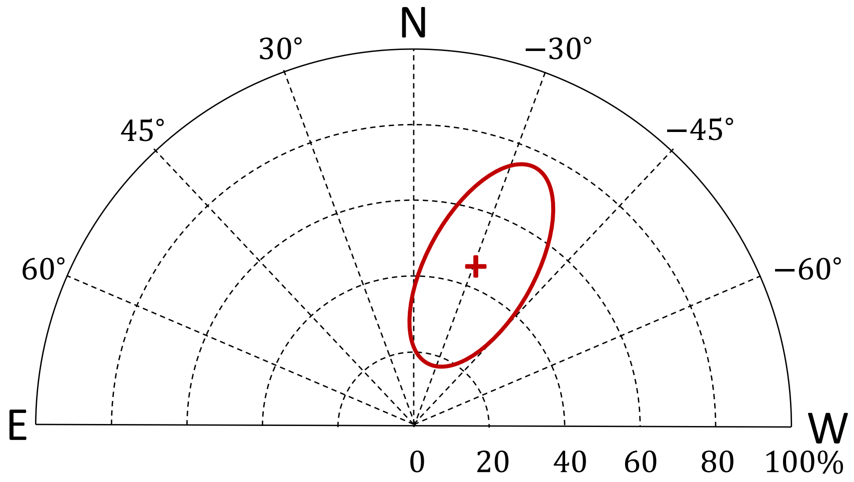

Polarization degree: $$\mathrm{PD} = \frac{1}{\mu}\frac{\mathcal{M}_{\max} - \mathcal{M}_{\min}}{\mathcal{M}_{\max} + \mathcal{M}_{\min}}$$

Polarization angle: $$\mathrm{PA} = \varphi_0$$

IXPE magnetar targets

- **AXP 4U 0142+61** (R.A. 01:46:22.41, DEC. 61°45'03''.2)
  - Cassiopeia – Distance: 3.6 kpc
  - January 31st – February 27th 2022 (840 ks)
  - Unabsorbed flux (2–10 keV): 6×10^{-11} erg cm^{-2} s^{-1}
- **AXP 1RXS J170849.0–4009100** (R.A. 17:08:46.3, DEC. –40°08'44''.6)
  - Scorpio – Distance: 5–10 kpc
  - September 19th – October 8th 2022 (837 ks)
  - Unabsorbed flux (2–10 keV): 2.4×10^{-11} erg cm^{-2} s^{-1}
- **SGR 1806–20** (R.A. 18:08:39.8, DEC. –20°24'26''.7)
  - Sagittarius – Distance: 8.7 kpc
  - March 22nd – April 13th 2023 (947 ks)
  - Unabsorbed flux (2–10 keV): 4×10^{-12} erg cm^{-2} s^{-1}

IXPE magnetar targets

- **AXP 1E 2259+586** (R.A. 23:01:08.8, DEC. 58°52’20’’.8)
  - Cassiopeia – Distance: 3.2 kpc
  - June 2nd – July 6th 2023 (1.2 Ms)
  - Unabsorbed flux (2–10 keV): 1.4×10^{-11} erg cm^{-2} s^{-1}

AXP 4U 0142+61

- Brightest among magnetars
- $B_{P\dot{P}} \approx 1.5 \times 10^{14}$ G
- Spectrum BB+PL
  - $kT_{\mathrm{BB}} = 0.471^{+0.004}_{-0.004}$ keV
  - $\Gamma = 3.69^{+0.05}_{-0.05}$
  - $\chi^2/\mathrm{dof} = 511.5/441$

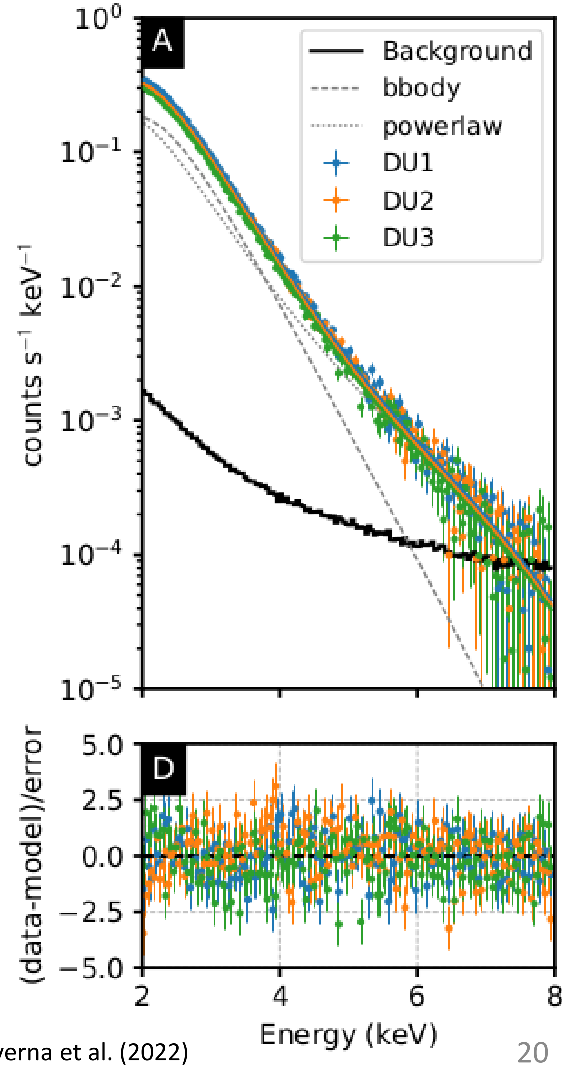

Taverna et al. (2022)

AXP 4U 0142+61

- Brightest among magnetars
- $B_{P\dot{P}} \approx 1.5 \times 10^{14}$ G
- Spectrum BB+PL
- Polarization measurement (2–8 keV):
  - PD = 13.5% (17σ) – PA ≈ 50° E
  - Complex behavior against photon energy

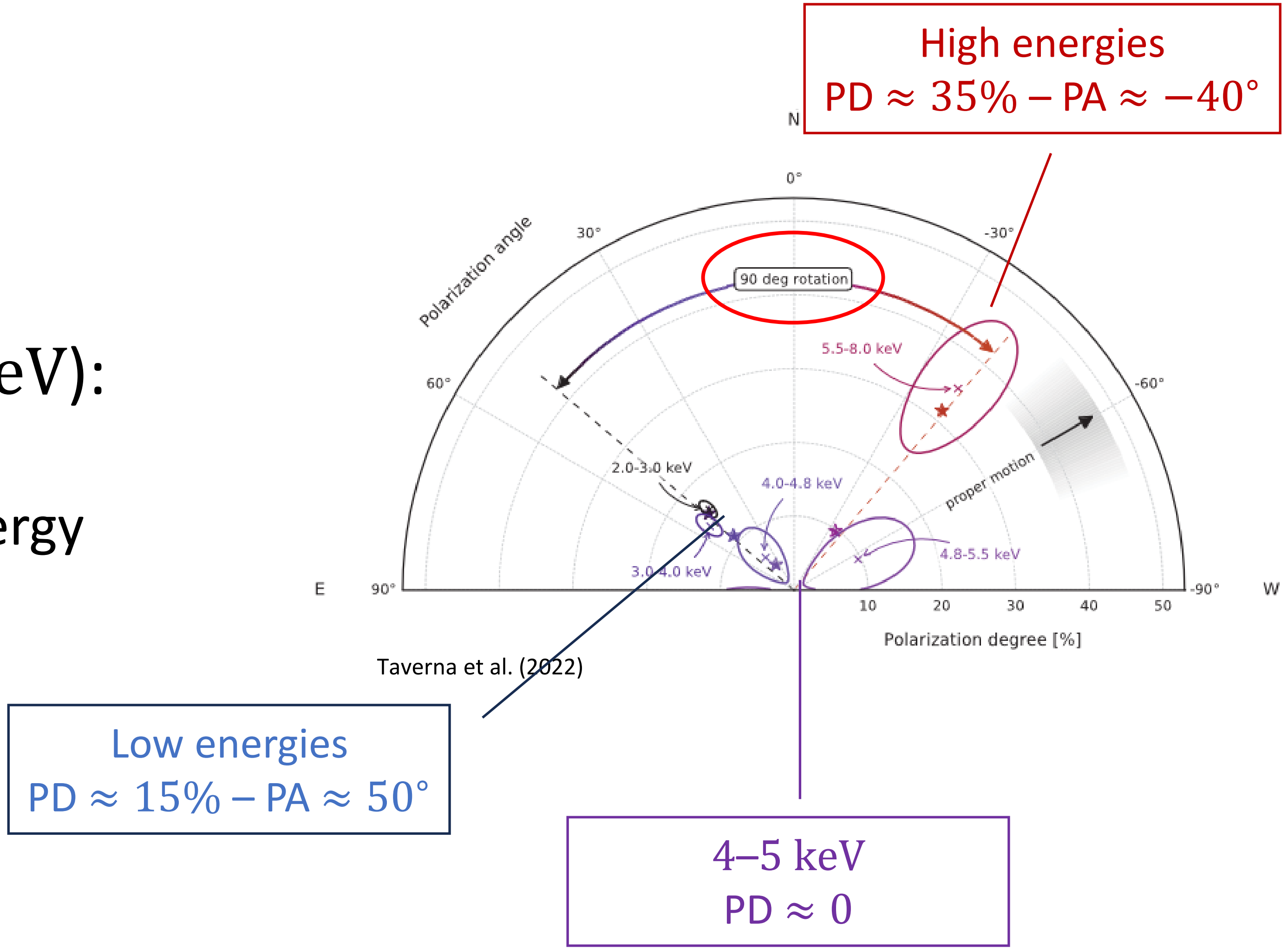

Taverna et al. (2022)

AXP 4U 0142+61

- Brightest among magnetars
- $B_{P\dot{P}} \approx 1.5 \times 10^{14}$ G
- Spectrum BB+PL
- Polarization measurement (2–8 keV):
  - PD = 13.5% (17σ) – PA ≈ 50° E
  - Complex behavior against photon energy

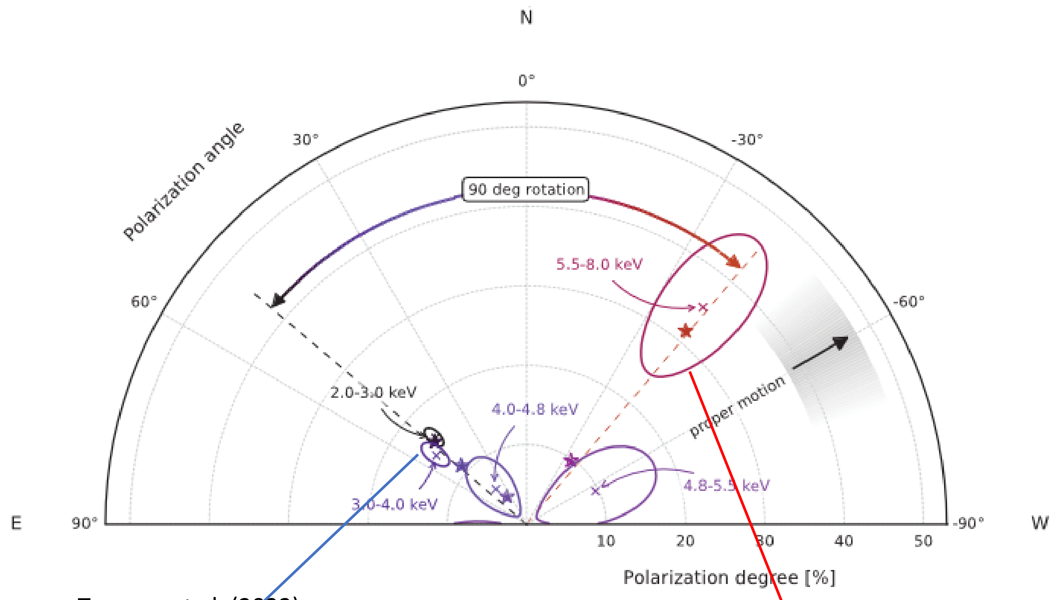

Taverna et al. (2022)

Thermal photons ⇒ O-mode

PL tail ⇒ X-mode

AXP 4U 0142+61

- Results are compatible with the magnetar model (Taverna+22)
  - $90°$-swing → X- and O-modes (ultra-strong B-fields $\gtrsim 10^{13}$ G independently from P-$\dot{P}$)
  - PD at high energies ($\approx 35\%$) → PL tail populated by RCS photons
  - According to the model RCS photons are X-mode → O-mode at low energies
  - Low PD + O-mode photons → condensed surface exposed (equatorial-belt emission geometry)

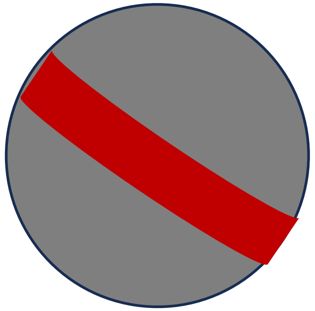

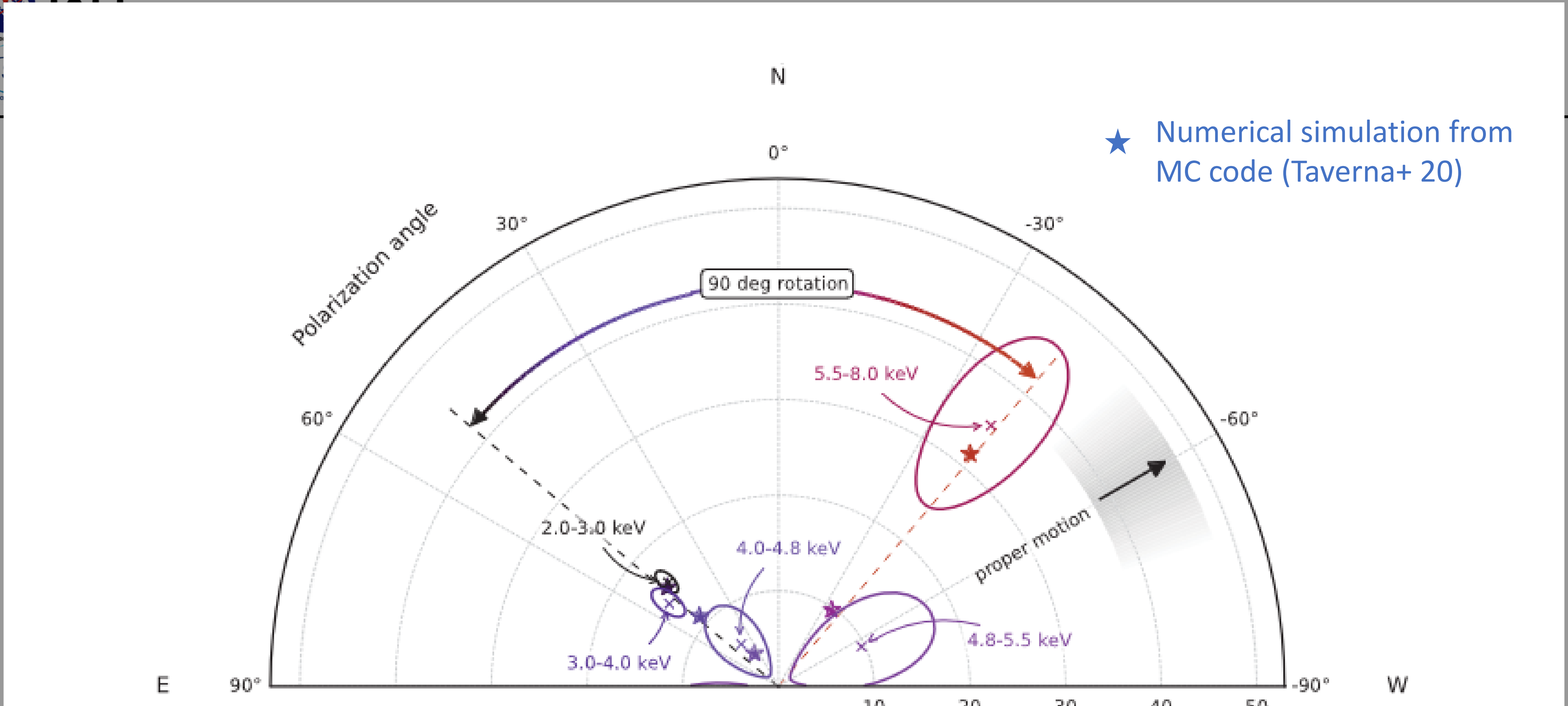

Taverna et al. (2022)

AXP 4U 0142+61

- Low phase-averaged PD (< 40%) ⇒ Vacuum birefringence cannot be probed
- Phase dependent results
  - PD is in-phase with the LC (determined at the surface)
  - PA is sinusoidal (RVM)

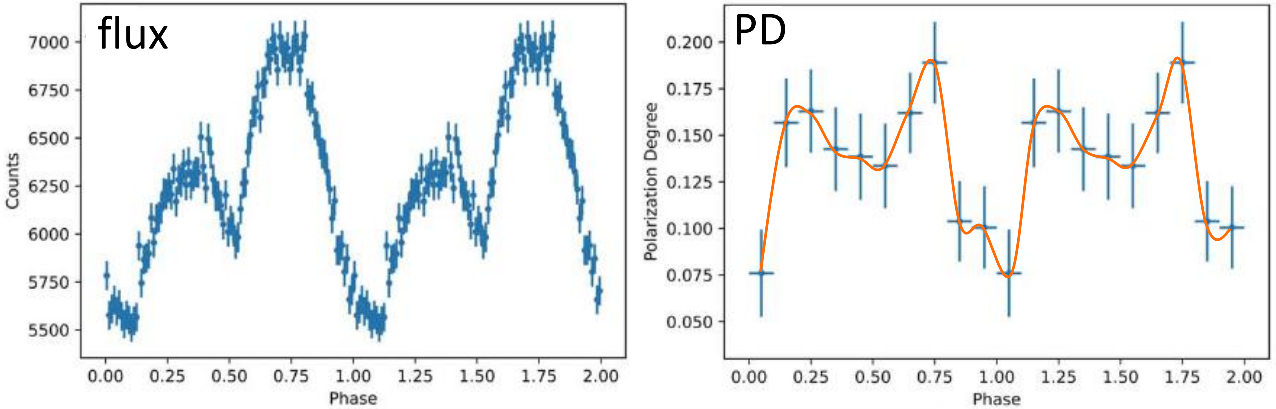

- RVM for extended regions holds for dipolar fields only
  - In the magnetar model B is dipolar only far away from the surface

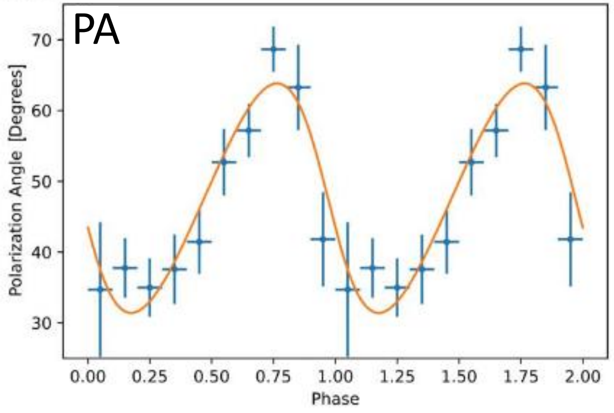

Taverna et al. (2022)

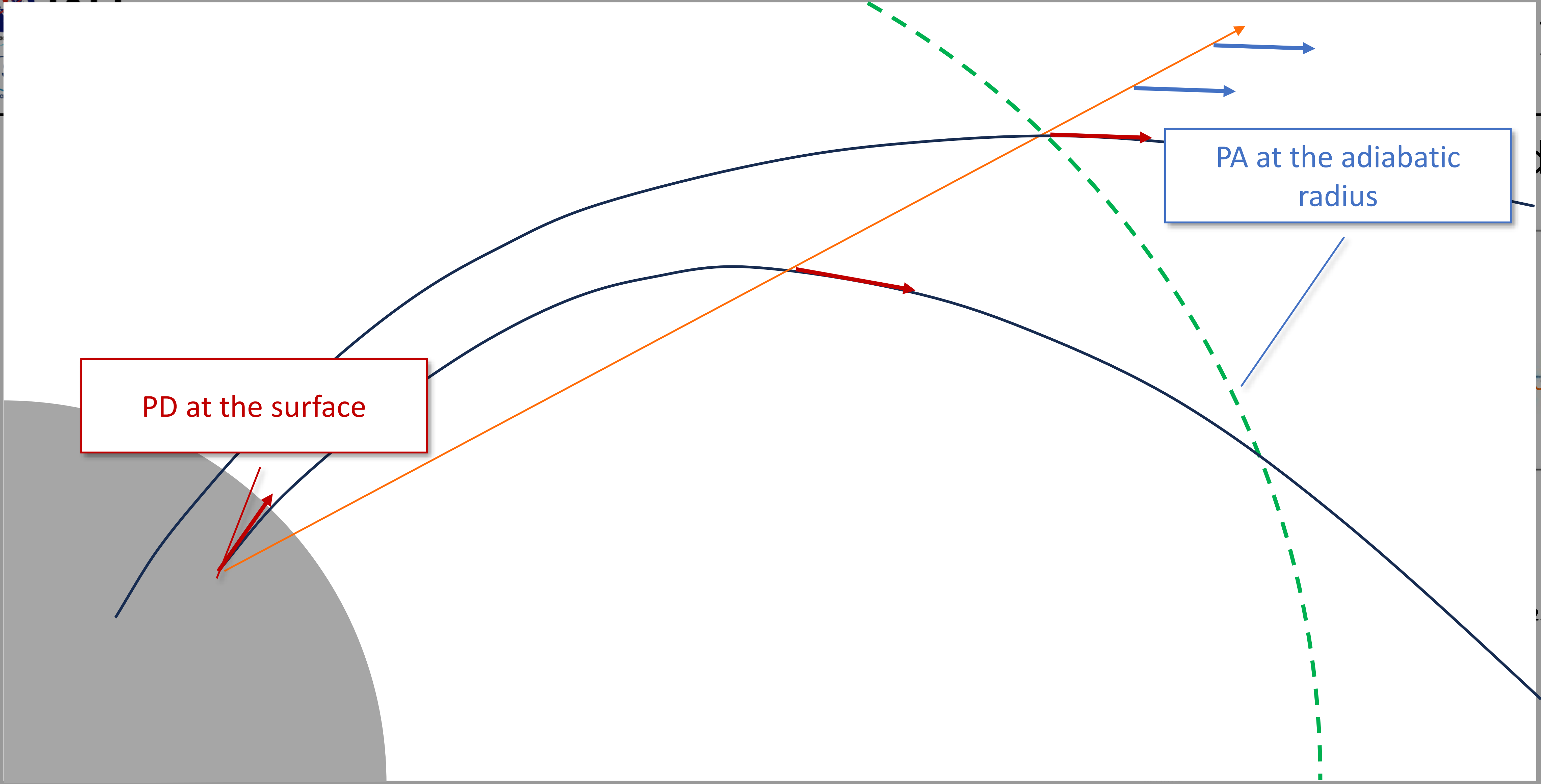
PD at the surface
PA at the adiabatic radius

AXP 1RXS J170849.0–4009100

- 2nd brightest magnetar
- $B_{P\dot{P}} \approx 5 \times 10^{14}$ G
- Spectrum BB+PL or BB+BB?
  - BB+PL – $kT_{\rm BB} = 0.454^{+0.007}_{-0.006}$ keV
    $\Gamma = 2.97^{+0.009}_{-0.056}$
    $\chi^2 = 410.8/408$ dof
  - BB+BB – $kT_{\rm BB_1} = 0.435^{+0.007}_{-0.007}$ keV
    $kT_{\rm BB_2} = 1.073^{+0.031}_{-0.029}$
    $\chi^2 = 405.8/408$ dof

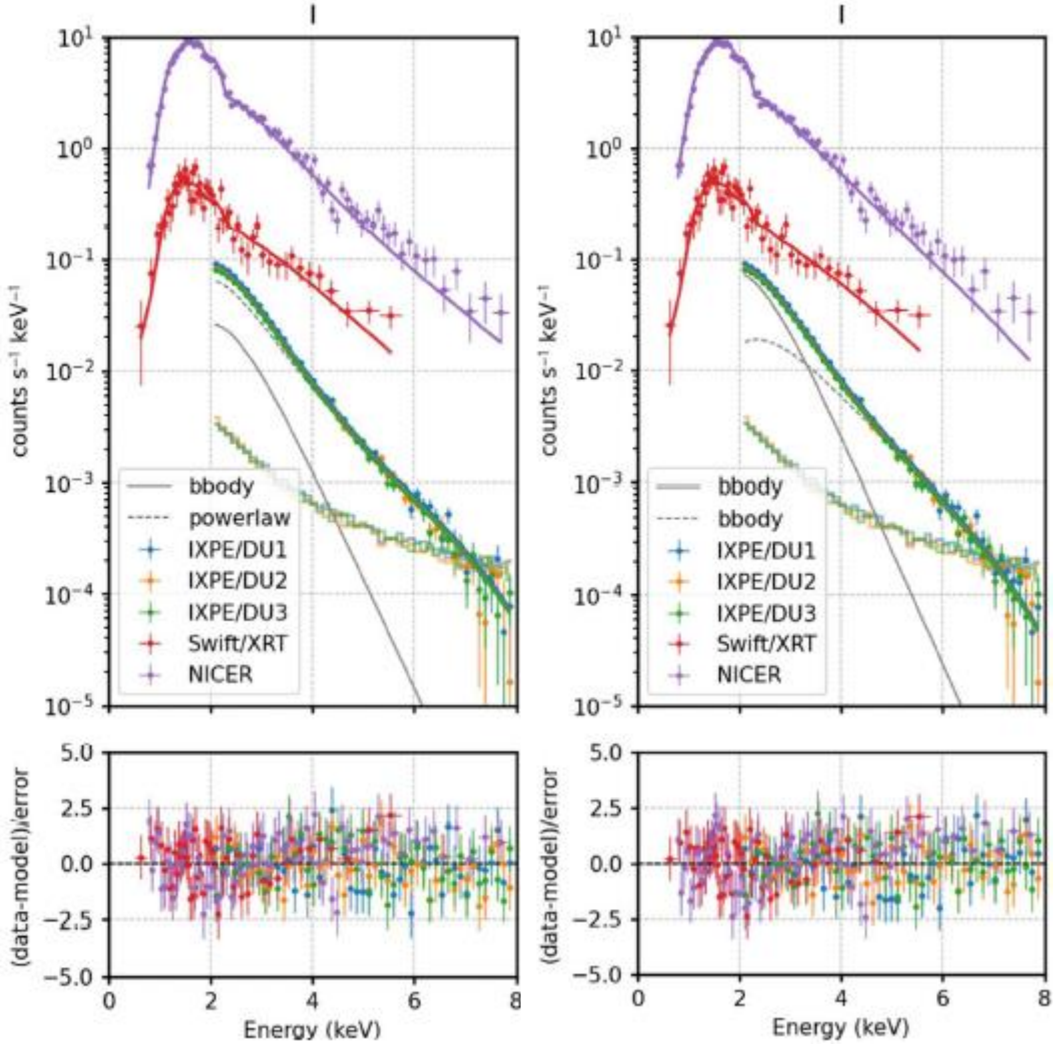

Zane et al. (2023)

AXP 1RXS J170849.0–4009100

- 2nd brightest magnetar
- $B_{P\dot{P}} \approx 5 \times 10^{14}$ G
- Spectrum BB+PL or BB+BB?
- Polarization measurement ($2\text{–}8$ keV):
  - PD $= 35\%$ (22.5σ) – PA $\approx 60°$ W
  - Polarization direction is kept in the IXPE band
  - PD at $6\text{–}8$ keV: $\approx 85\%$ ($\text{MDP}_{99} = 50\%$)
    <u>the highest measured so far!</u>

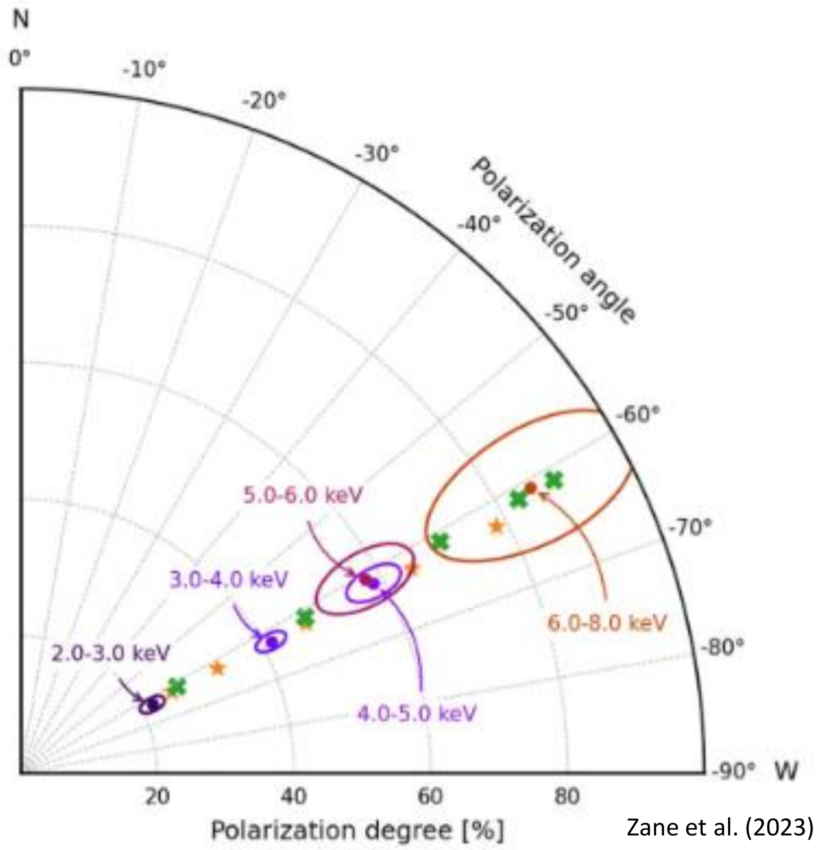

Zane et al. (2023)

AXP 1RXS J170849.0–4009100

- Theoretical interpretation
  - high PD points towards plasma reprocessing → NS atmosphere

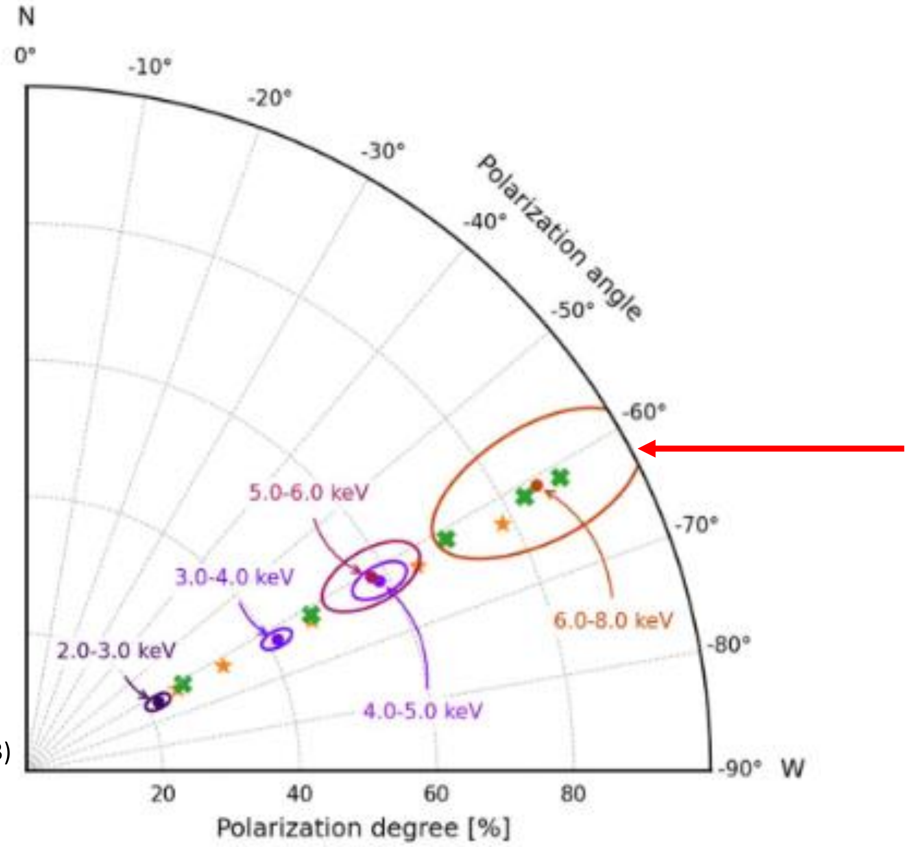

Zane et al. (2023)

AXP 1RXS J170849.0–4009100

- Theoretical interpretation
  - high PD points towards plasma reprocessing → NS atmosphere
  - PD at high energies too large for RCS ($\approx 33\%$) → BB+BB (2 distinct thermal regions)

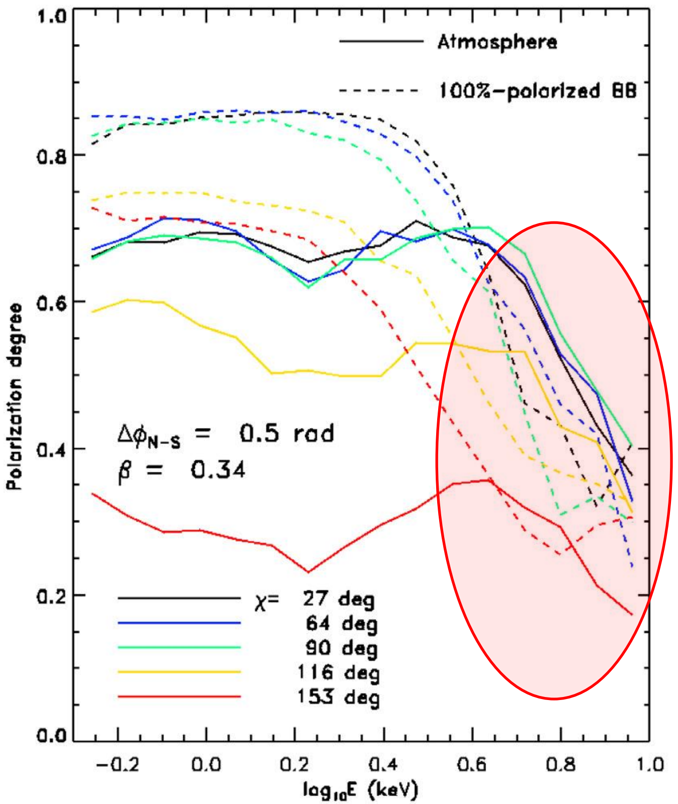

Taverna et al. (2020)

AXP 1RXS J170849.0–4009100

- Theoretical interpretation
  - high PD points towards plasma reprocessing → NS atmosphere
  - PD at high energies too large for RCS ($\approx 33\%$) → BB+BB (2 distinct thermal regions)
  - PD at low energies too small for atmosphere → condensed surface

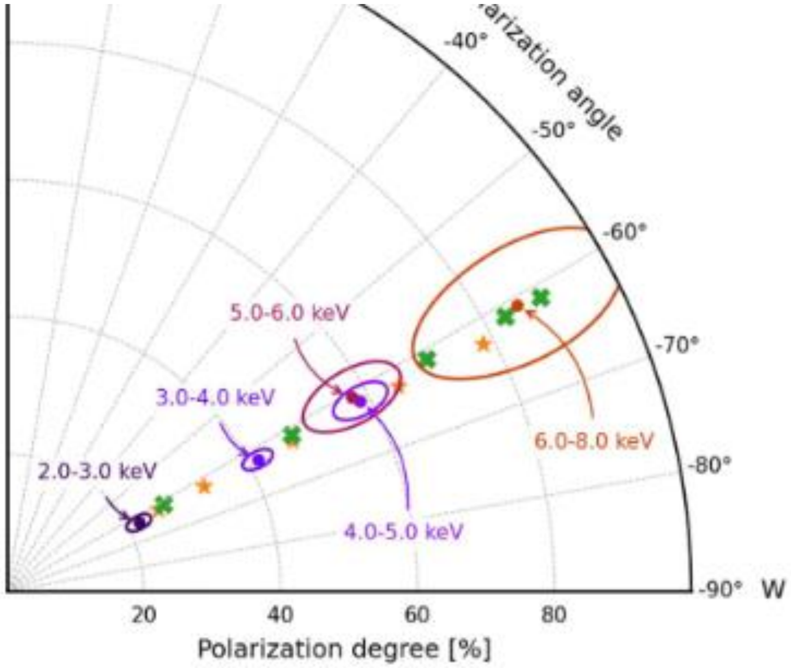

Zane et al. (2023

AXP 1RXS J170849.0–4009100

- Theoretical interpretation
  - high PD points towards plasma reprocessing → NS atmosphere
  - PD at high energies too large for RCS ($\approx 33\%$) → BB+BB (2 distinct thermal regions)
  - PD at low energies too small for atmosphere → condensed surface

⇓

Phase transition across the surface

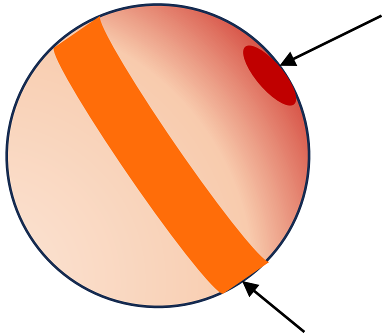

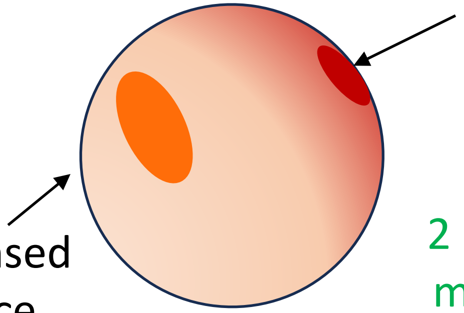

IXPE Imaging X-Ray Polarimetry Explorer

AXP 1RXS J170849.0–4009100

- Phase-dependent results are coherently explained by the models

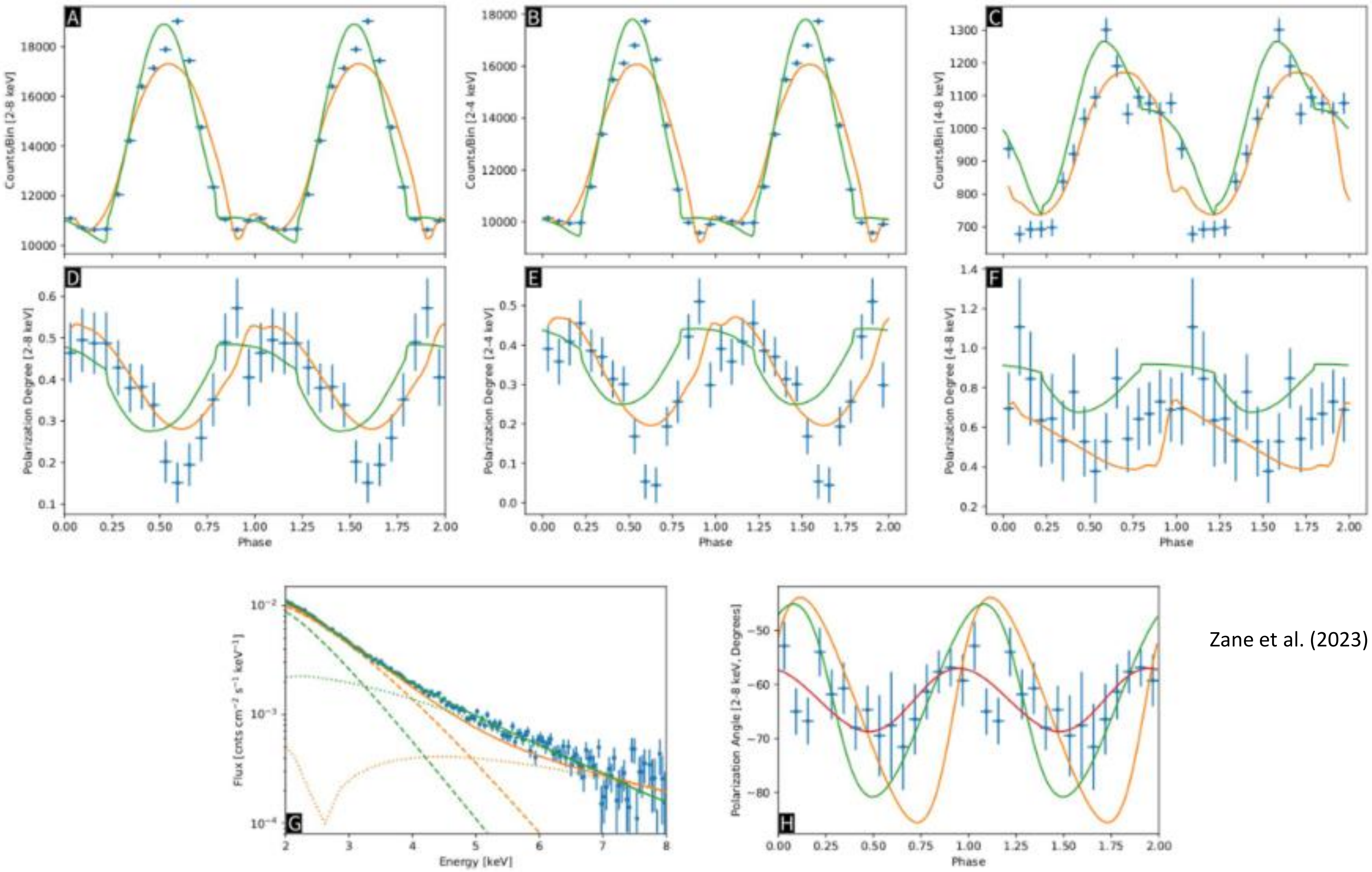

CAP+BELT model

2 CAPS model

Zane et al. (2023)

SGR 1806–20

- Emitted the strongest giant flare ever detected (December 27, 2004)
- $B_{P\dot{P}} \approx 8 \times 10^{14}$ G (strongest B-field)
- Obsereved during an active phase

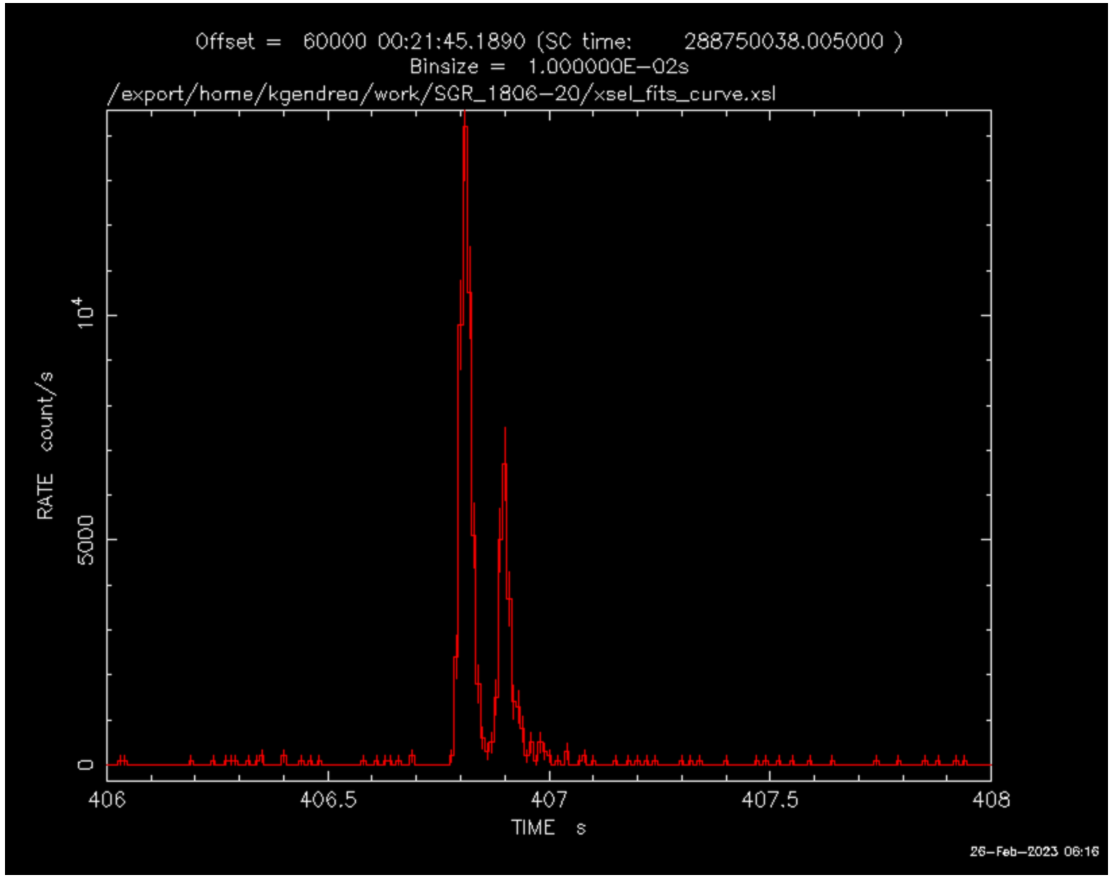

Courtesy of G. Israel

SGR 1806–20

- Emitted the strongest giant flare ever detected (December 27, 2004)
- $B_{P\dot{P}} \approx 8 \times 10^{14}$ G (strongest B-field)
- Obsereved during an active phase
- Unexpectedly low flux level (1/10 than tabulated)
- Contamination by solar flares during IXPE observation

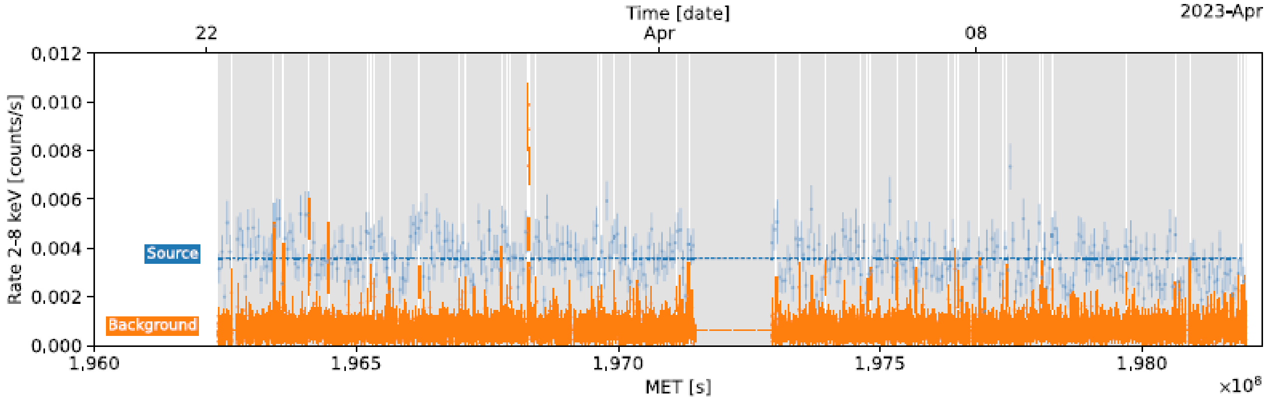

SGR 1806–20

- Spectral and timing analysis from XMM DDT observation
  - BB+PL spectral decomposition ($kT_{\rm BB} = 0.59 \pm 0.04\ {\rm keV}, \Gamma = 1.7 \pm 0.1$)
  - Double-peaked pulse profile ($\rm P.F. \approx 5\%$)

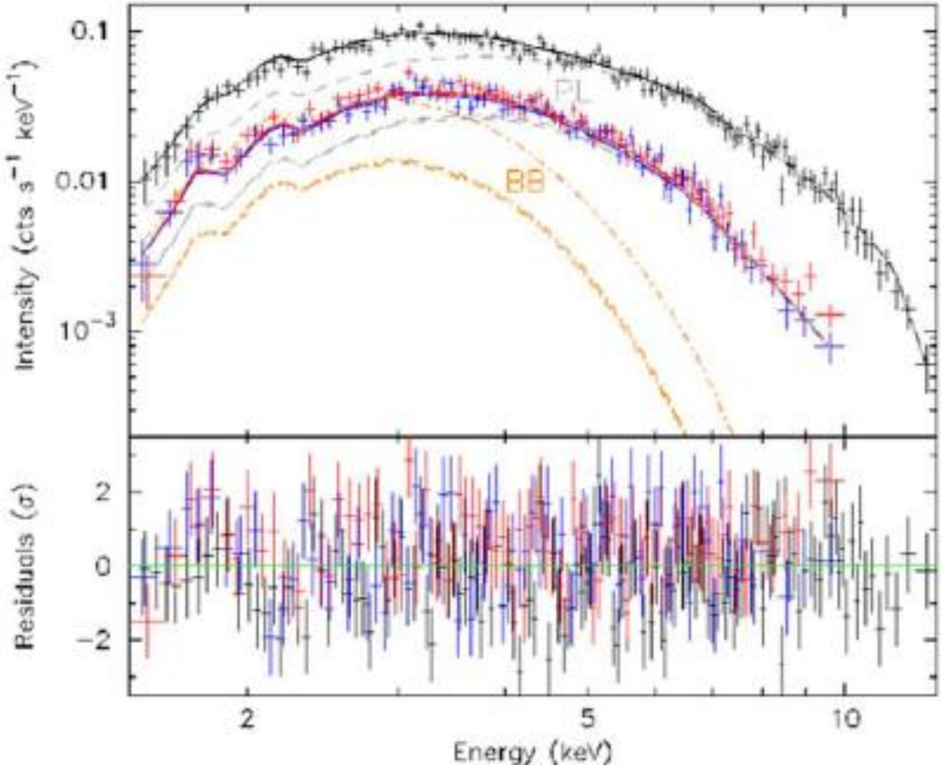

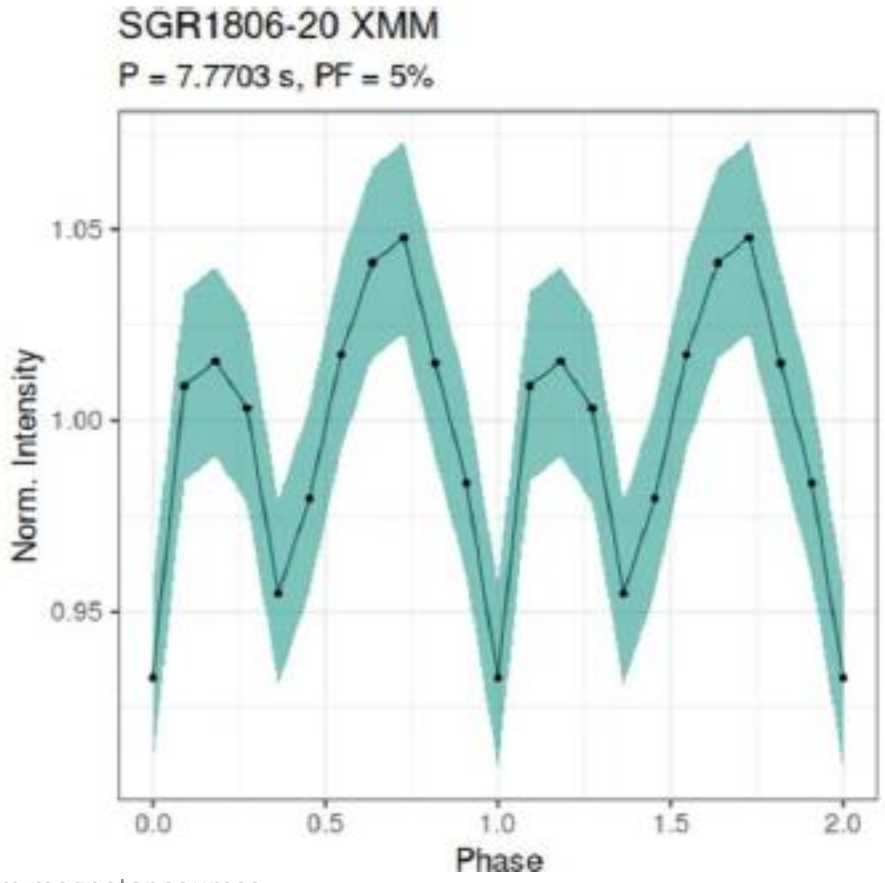

Turolla et al. (2023)

SGR 1806–20

- Spectral and timing analysis from XMM DDT observation
  - BB+PL spectral decomposition ($kT_{\rm BB} = 0.59 \pm 0.04$ keV, $\Gamma = 1.7 \pm 0.1$)
  - Double-peaked pulse profile ($\rm P.F. \approx 5\%$)

- Marginally significant IXPE measurement
  - Phase- and energy-integrated PD (5.7%) well below $\rm MDP_{99}$ ($\approx 20\%$)
  - Energy-dependent PD (99% c.l.)
    $\lesssim 24\%$ (2–4 keV)
    $\approx 32\%$ (4–5 keV, 99% c.l.)
    $\lesssim 55\%$ (5–8 keV)

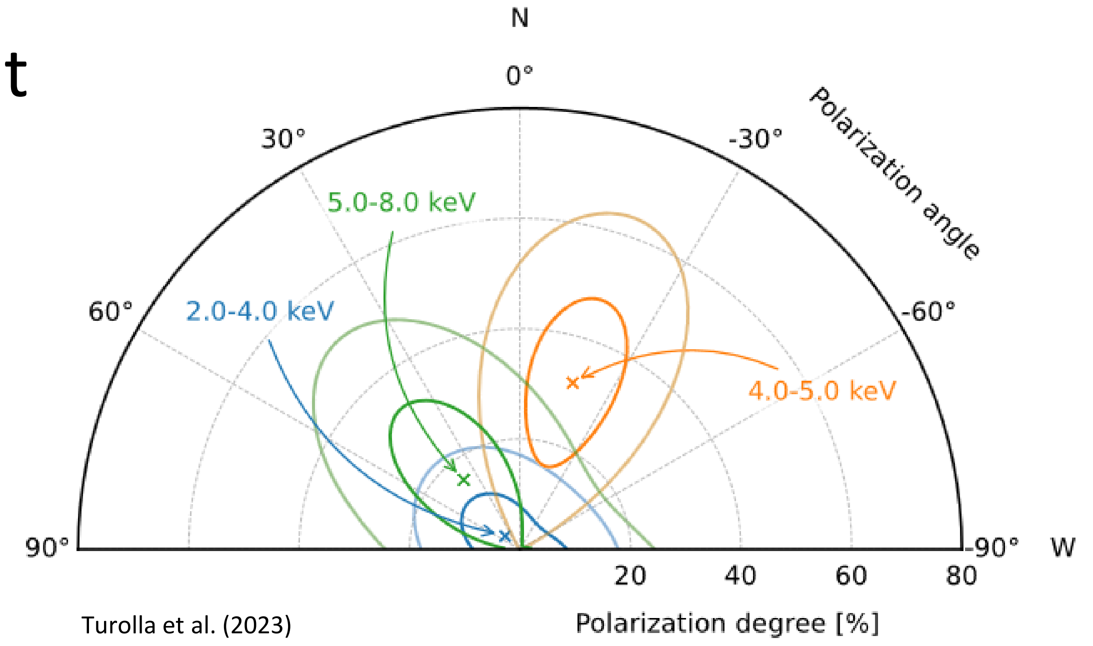

Turolla et al. (2023)

- Thoretical interpretation
  - Limited by the non-significant polarization measurement
  - IXPE observations are not incompatible with emission from a condensed region of the surface reprocessed by RCS (4U like)

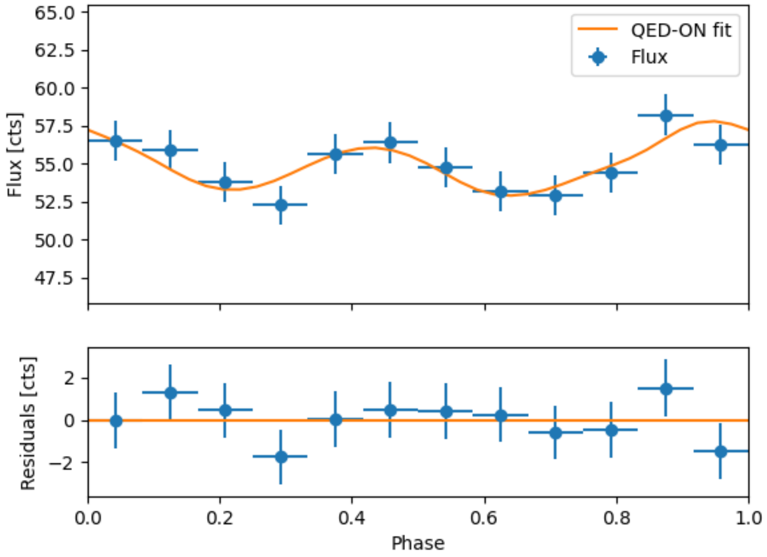

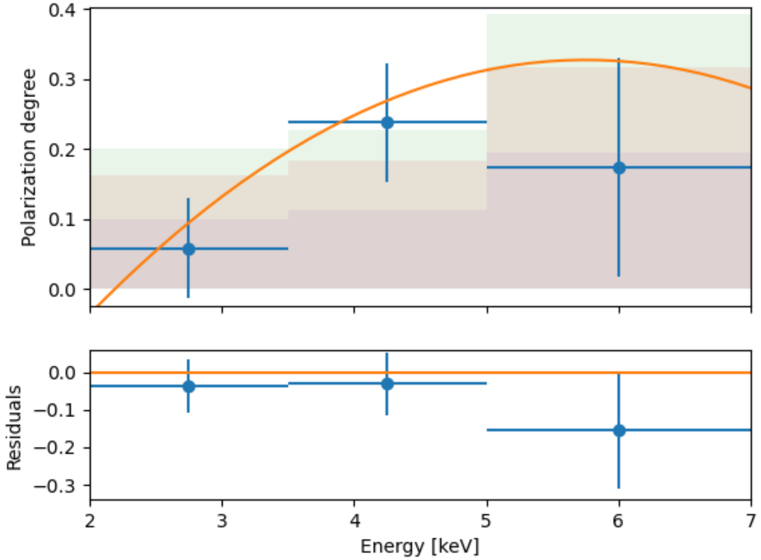

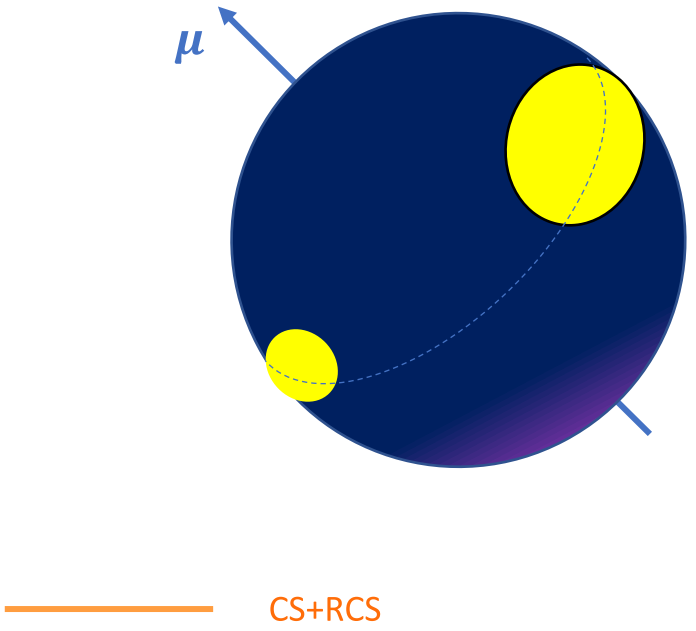

AXP 1E 2259+586

- XMM & NICER observations
- $B_{P\dot{P}} \approx 6 \times 10^{13}$ G (not so much)
- Spectral fit BB+PL is not good enough → adding an absorption line (Pizzocaro+19) improves the fit

	$kT_{\rm BB}$ (keV)	Γ	$E_{\rm line}$ (keV)	$\sigma_{\rm line}$ (keV)	χ^2/dof
XMM	0.44 ± 0.01	4.09 ± 0.08	$0.96^{+0.07}_{-0.18}$	$0.23^{+0.10}_{-0.06}$	94.1/93
IXPE	0.43 ± 0.01	4.36 ± 0.09	frozen	frozen	138.0/147

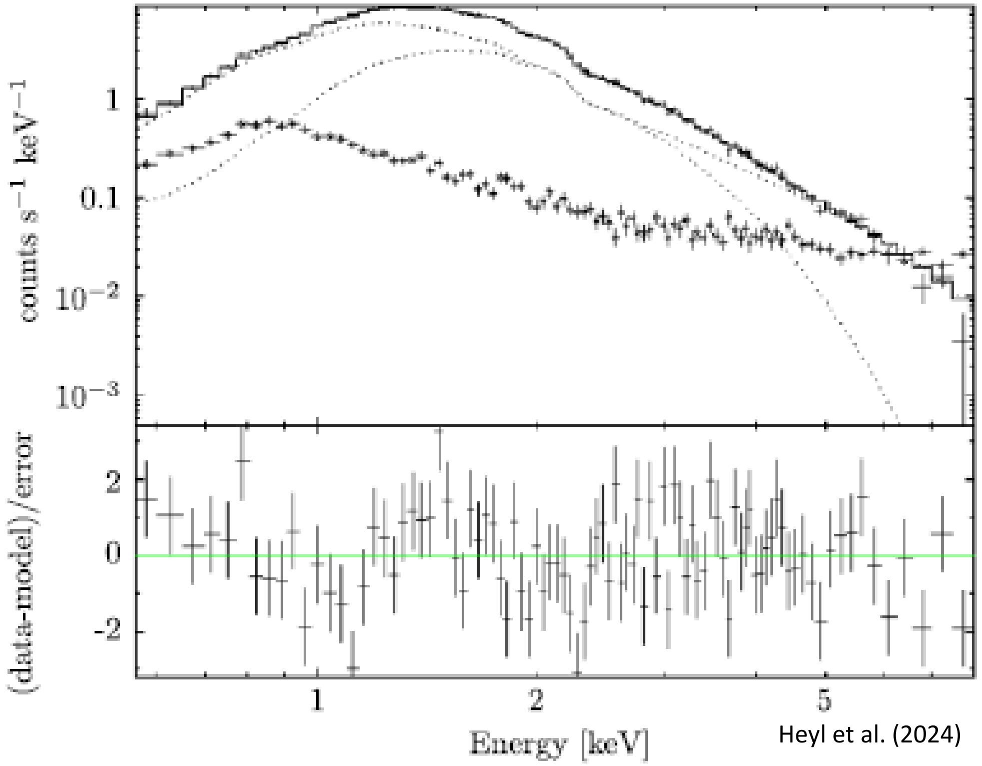

Heyl et al. (2024)

AXP 1E 2259+586

- Peculiar phase-dependent behavior
  - Polarization up to $\approx 30\%$ (well above MDP_{99}) at particular phases (corresponding to the rise and maximum of the primary LC peak)
  - Secondary peak basically unpolarized
  - PA well fitted by a RVM in which photons are assumed to change mode (from O- to X- and vice versa)

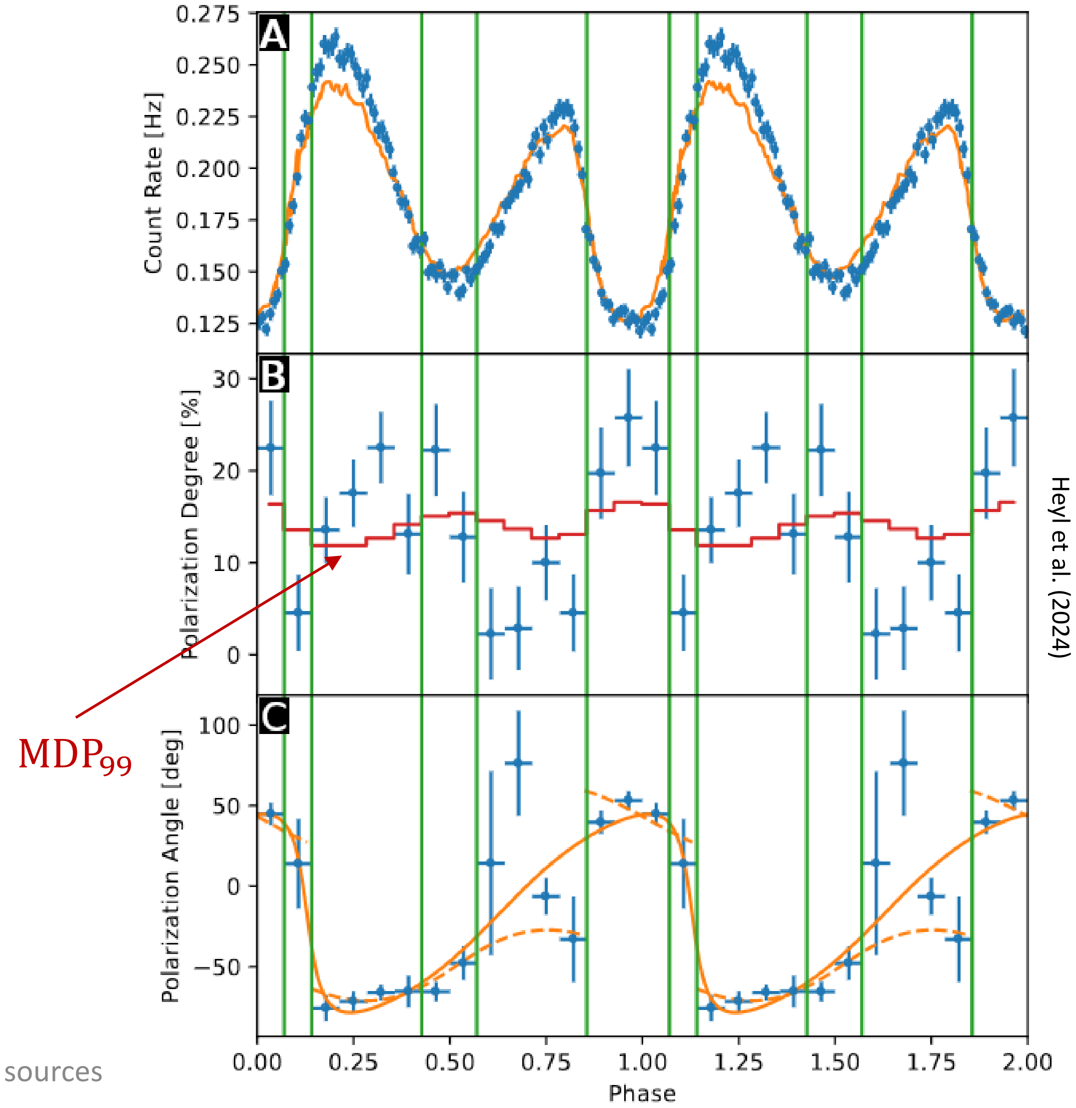

Heyl et al. (2024)

AXP 1E 2259+586

- Theoretical interpretation (in terms of the magnetic-loop model)
  - Two emitting regions (condensed surface, O-mode dominated)
  - One of the two spot covered by a «magnetic loop» crossed by plasma particles
  - Primary photons reprocessed by RCS onto protons (Pizzocaro+19, Tiengo+13)

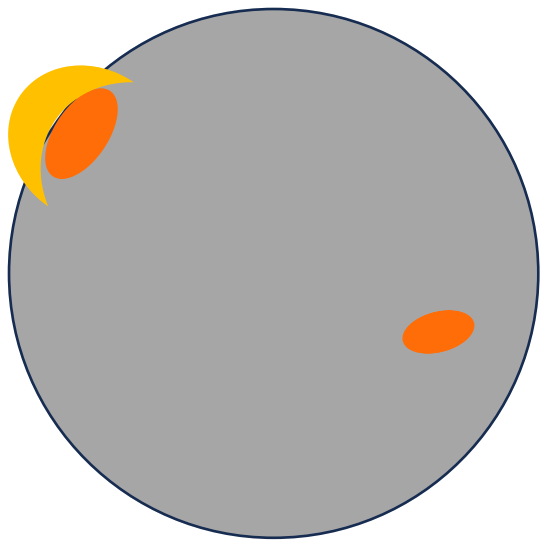

AXP 1E 2259+586

- Theoretical interpretation (in terms of the magnetic-loop model)

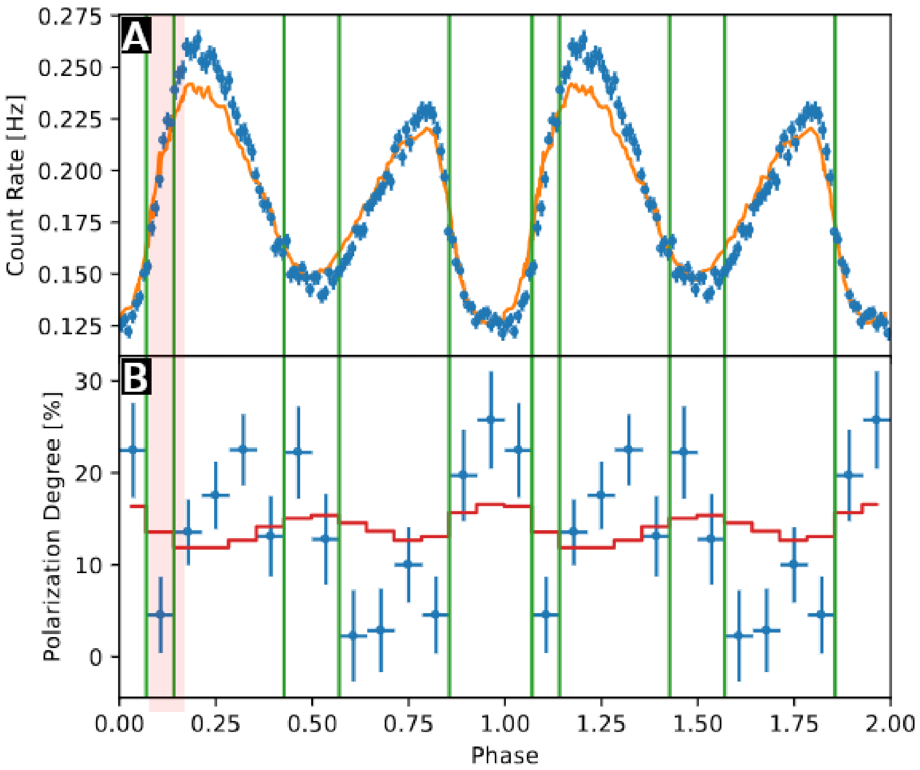

1st rise

- unscattered (O-mode) photons (lowly polarized) are directly intercepted
- scattered photons are deviated away from the LOS

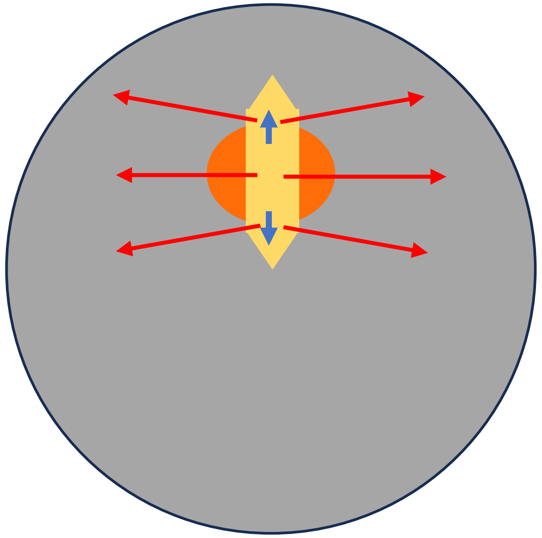

AXP 1E 2259+586

- Theoretical interpretation (in terms of the magnetic-loop model)

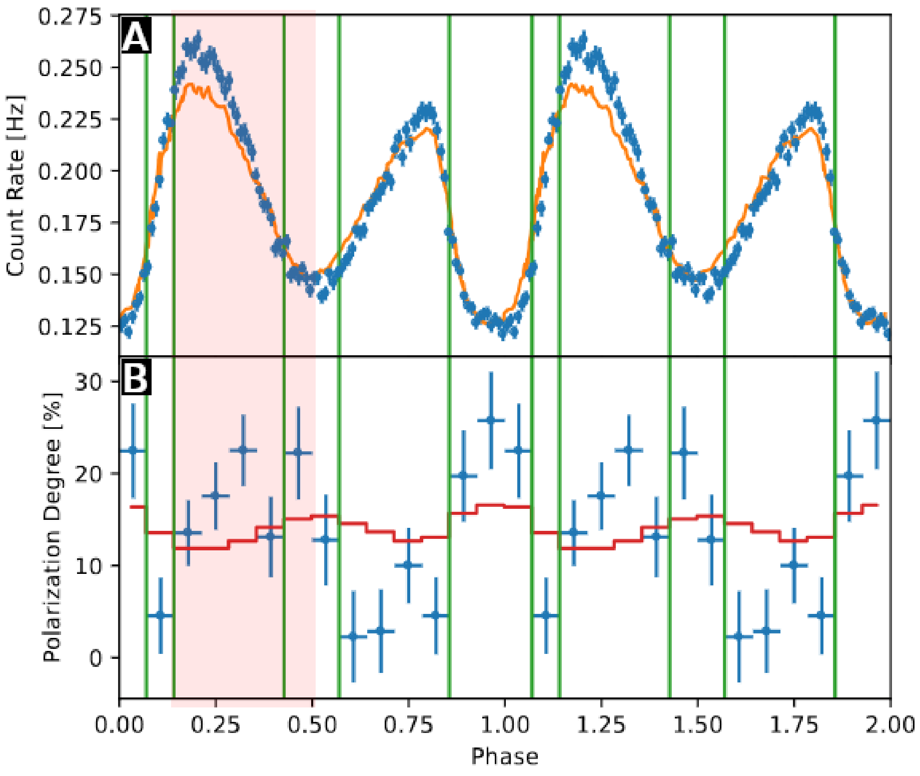

1st peak

- scattered X-mode photons are now intercepted (with also primary O-mode ones from the underlying spot → peak in the flux)
- polarization increases
- contamination from O-mode condensed-surface photons prevent PD to reach 33%

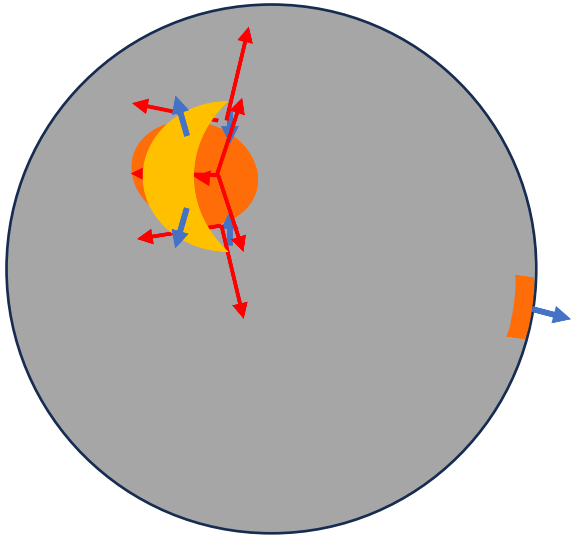

AXP 1E 2259+586

- Theoretical interpretation (in terms of the magnetic-loop model)

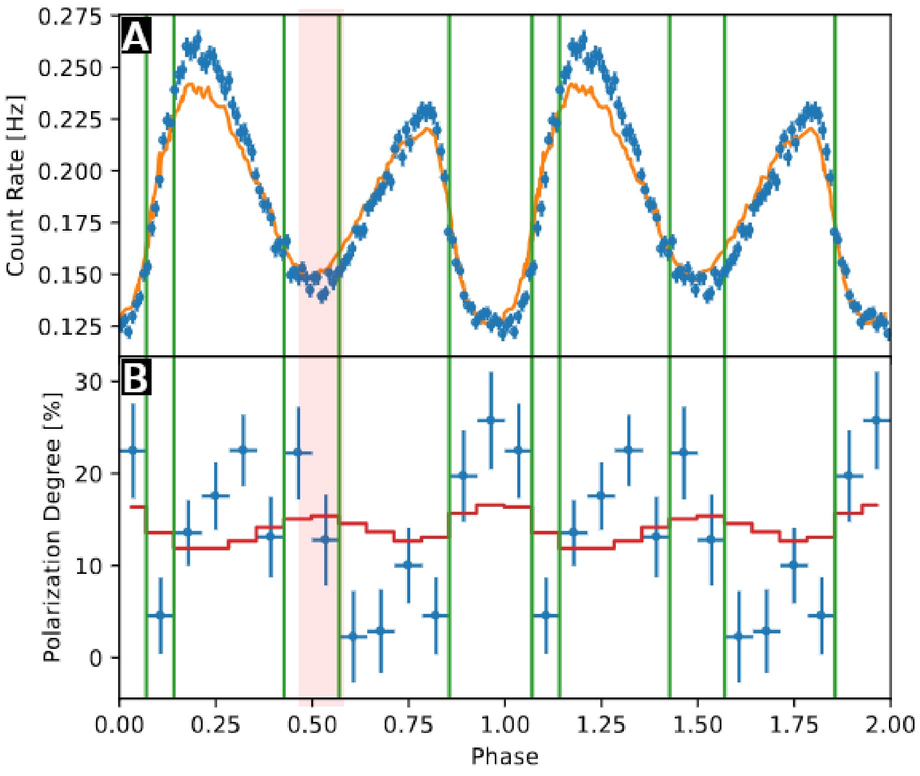

Little dip

- the larger spot starts to be hidden behind (only a fraction of mildly polarized photons are observed)
- the secondary spot (with no loop) enters in view (emitting low-polarized O-mode photons)

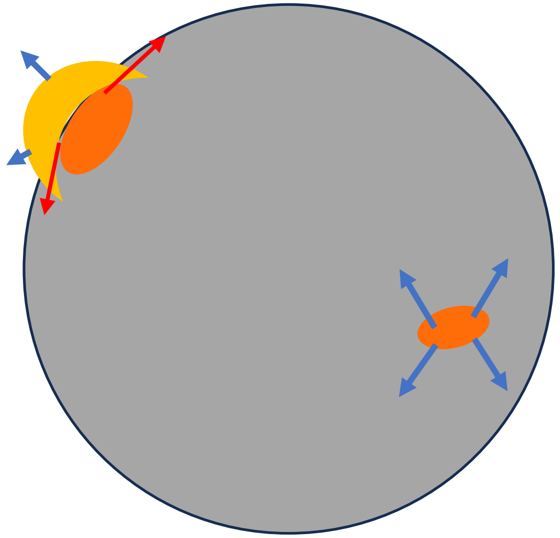

AXP 1E 2259+586

- Theoretical interpretation (in terms of the magnetic-loop model)

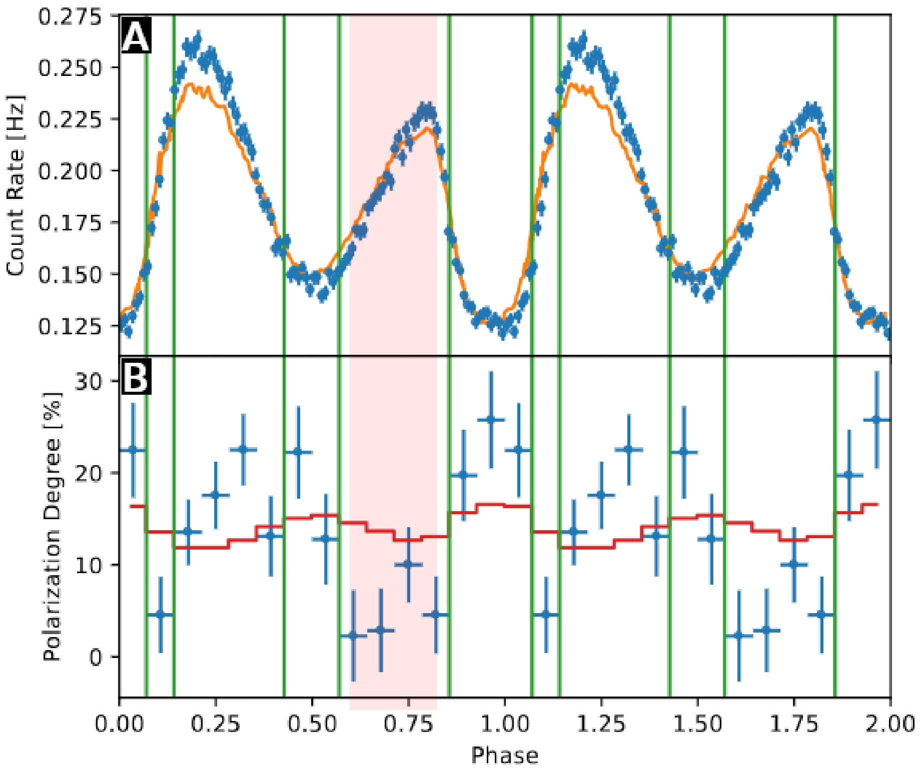

2nd peak

- the secondary spot is fully in view (peak in the flux)
- only condensed-surface photons collected (O-mode, polarized at no more than 10–15%)

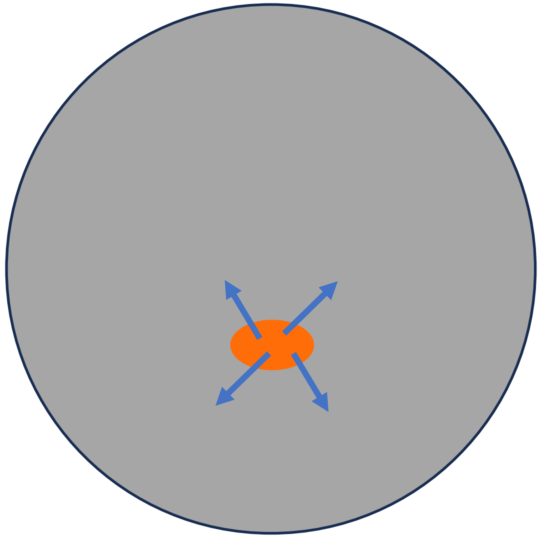

AXP 1E 2259+586

- Theoretical interpretation (in terms of the magnetic-loop model)

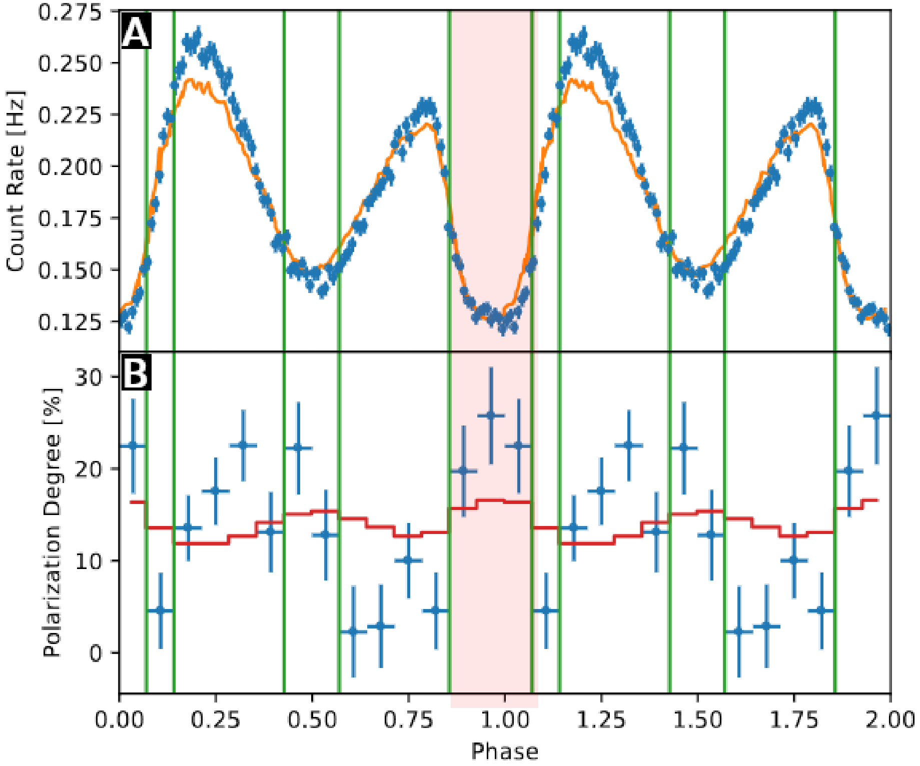

Big dip

- secondary spot photons are not in view
- the primary peak returns in view
- X-mode scattered photons along the LOS are intercepted first (minimum in the flux, maximum in PD)

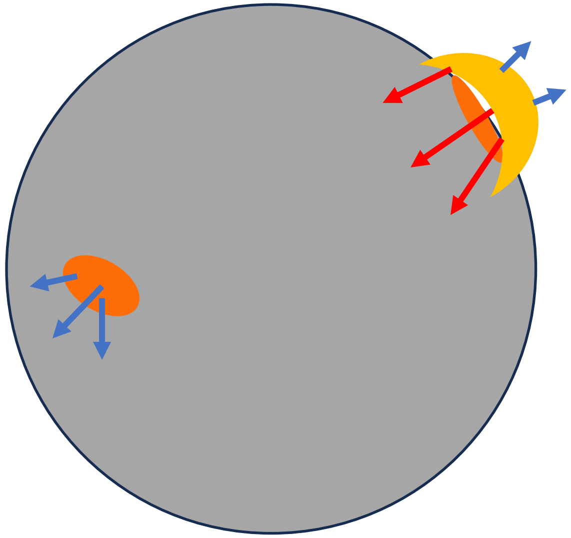

IXPE Imaging X-Ray Polarimetry Explorer

Conclusions

- X-ray polarimetry on magnetar sources complemented information from spectral and timing analysis
- Detection of photons polarized in two normal modes in the same source (4U 0142) confirmed the presence of strong magnetic fields ($\gtrsim 5 \times 10^{13}$ G)
- Energy-dependent PD and PA allowed to confirm the expectations of the RCS model (at least in some persistent sources)
- Phase-dependent PD and PA provided a first hint that vacuum birefringence effects are at work around magnetars
- Further magnetars should be explored in polarized X-rays (persistent and transient in outburst)